

Collective bath coordinate mapping of “hierarchy” in hierarchical equations of motion

Tatsushi Ikeda^{1,*} and Akira Nakayama¹

¹*Department of Chemical System Engineering, The University of Tokyo, Tokyo 113-8656, Japan*
(Dated: December 21, 2021)

The hierarchical equations of motion (HEOM) theory is one of the standard methods which give exact evaluations of dynamics coupled to harmonic oscillator environments. The theory is, however, numerically demanding because of its hierarchy, i.e., a set of auxiliary elements introduced to capture non-Markovian and non-perturbative effects of environments; When a system-bath coupling becomes strong to some extent, the required computational resources and precisions get beyond the regime we can handle. In this article, we present a new representation of the HEOM theory, in which the hierarchy is mapped into a continuous space of collective bath coordinate and several auxiliary coordinates. The new approach is more stable and efficient than the original HEOM theory, particularly when a strong system-bath coupling exists. We demonstrate that this approach is suitable for treating a vibronic system model coupled to environments.

This article may be downloaded for personal use only.

I. INTRODUCTION

Theories describing open quantum dynamics are widely used to understand chemical and biological phenomena because energy transfers between systems and environments have essential roles in their behavior [1, 2]. In descriptions for ultra-fast phenomena, such as those observed in recent advanced spectroscopy experiments [3–8], we sometimes need to employ open quantum theories that can treat non-Markovian non-perturbative effects of environments. When the dynamics of the system are fast to some extent, the timescale of the dynamics could be similar to the correlation timescales of the surrounding environments, and then we cannot employ the Markovian approximation. Many theories have been developed to capture the system-environment coupling effects [9–16], and the hierarchical equations of motion (HEOM) theory is one of the standards in such theories nowadays [17–22]. The HEOM theory is used not only to describe quantum dynamics [23–31], but also to give reference calculations for developments of theories [32, 33].

The HEOM theory was originally developed by Tanimura and Kubo to describe the dynamics of an open quantum system coupled to a high-temperature Drude bosonic environment (bath) which could be characterized by a single-exponential environment correlation function [17]. Many extensions have been performed to treat more general situations. For example, treatments for the low-temperature quantum effects come from the Bose–Einstein distribution function [34–36], for multi-exponential bath correlation functions [37–42], and for non-exponential correlation functions [19–21]. However, the theories are numerically demanding because of their hierarchical structures, i.e., a set of auxiliary elements introduced to capture non-Markovian and non-perturbative effects of environments. The stronger a

system-bath coupling in the model system, the larger hierarchy we need to obtain converged calculations. When the coupling becomes strong to some extent, the required computational resources and precisions get beyond the regime we can handle. As seen in numerical examples in this paper, coupling easily reaches the extent, especially in the case of vibronic systems.

In this article, we present a new representation of the HEOM theory, in which the hierarchy is mapped into a continuous space of collective bath coordinate and several auxiliary coordinates. The new approach is more stable and efficient than the original HEOM theory, particularly when a strong system-bath coupling exists. It has already been shown that the HEOM for a high-temperature Drude bosonic bath is equivalent to a modified version of the Zusman equation [17, 43–45], and the HEOM for undamped bath modes is equivalent to the Wigner transport equation coupled to the system [46–48]. In this paper, we show treatment for damped bath correlation functions, including quantum low-temperature effects. It is interesting that our exact derivation gives a quantum Fokker–Planck equation for auxiliary modes coupled to the system [18, 30, 45, 49–52]; An idea that uses similar auxiliary modes is shown in Refs. 33 and 53, but a Lindblad form is assumed there.

The organization of this paper is as follows; In section II, we show mapping the hierarchy in the HEOM into a continuous coordinate space and construct the collective bath coordinate representation for a Drude spectral density model. In section III, we present numerical results for cases of a vibronic system and two-level system, which show the pros and cons of our theory. Finally, section IV is devoted to concluding remarks.

II. THEORY

While it is possible to construct our approach without passing the HEOM theory, we derive our approach from the HEOM theory. This derivation clarifies the re-

* t.ikeda@chemsys.t.u-tokyo.ac.jp

lation between the two theories and gives another aspect of the physical meanings of the hierarchical elements in the HEOM theory.

A. Hamiltonian

We consider a system linearly coupled to a harmonic oscillator bath. Here, we assume that the system–bath interaction is characterized by a single system subspace operator \hat{V} for simplicity. The total Hamiltonian of the system is expressed as

$$\hat{H}^{\text{tot}} \equiv \hat{H} + \hat{H}^{\text{bath}} + \hat{H}^{\text{int}}, \quad (1)$$

where \hat{H} , \hat{H}^{bath} , and \hat{H}^{int} are the Hamiltonian operators of the system, bath, and interaction, respectively. The bath Hamiltonian reads

$$\hat{H}^{\text{bath}} \equiv \sum_{\xi} \frac{\hbar\omega_{\xi}}{2} (\hat{p}_{\xi}^2 + \hat{x}_{\xi}^2), \quad (2a)$$

where \hat{x}_{ξ} , \hat{p}_{ξ} , and ω_{ξ} are the dimensionless coordinate, conjugate momentum, and characteristic frequency of the ξ th bath mode, and the interaction Hamiltonian is expressed as

$$\hat{H}^{\text{int}} \equiv -\hbar\hat{V} \sum_{\xi} g_{\xi} \hat{x}_{\xi} = -\hbar\hat{V} \hat{X} \quad (2b)$$

where g_{ξ} is the coupling strength between the system and the ξ th bath mode. We have introduced the collective bath coordinate $\hat{X} \equiv \sum_{\xi} g_{\xi} \hat{x}_{\xi}$. Note that the bath modes are coupled to the system only through the coordinate \hat{X} .

B. Bath

We assume that the total density operator at $t = t_0$ can be written as

$$\hat{\rho}^{\text{tot}}(t_0) = \hat{\rho}(t_0) \otimes \hat{\rho}_{\text{eq}}^{\text{bath}}, \quad (3)$$

where $\hat{\rho}(t_0)$ is the reduced density operator of the system subspace and $\hat{\rho}_{\text{eq}}^{\text{bath}}$ is the bath equilibrium density operator at temperature T , i.e., $\hat{\rho}_{\text{eq}}^{\text{bath}} = e^{-\beta\hat{H}^{\text{bath}}} / \mathcal{Z}^{\text{bath}}$. Here, $\mathcal{Z}^{\text{bath}}$ is the partition function of the bath and $\beta \equiv 1/k_{\text{B}}T$ is the inverse temperature divided by the Boltzmann constant k_{B} . In open quantum theories, including the HEOM theory, we are mainly concerned with dynamic properties of the reduced density operator at $t > t_0$, defined as

$$\hat{\rho}(t) \equiv \text{Tr}^{\text{bath}}\{\hat{\rho}^{\text{tot}}(t)\}, \quad (4)$$

where $\text{Tr}^{\text{bath}}\{\dots\}$ is the trace over the bath subspace.

Note that the factorized initial condition Eq. (3) is merely temporarily introduced to evaluate time evolution of the reduced system and is not a restriction of

numerical calculations; In the case that we need to start from the correlated thermal equilibrium state of the total system, one of the possible prescriptions is simulating time evolution of the system from time $t = t_0$ with the temporal initial state Eq. (3) to a sufficiently long time $t = t_i \gg t_0$ at which the total system reaches the thermal equilibrium state. Then, we can regard the state at $t = t_i$ as the initial state of the following calculations [18, 40]. For the other possible prescriptions, see Refs. 54–56.

In the case of a harmonic environment model, all the effects of the set of bath modes to system dynamics are entirely characterized by its spectral density, defined as

$$\mathcal{J}(\omega) \equiv \pi \sum_{\xi} \frac{g_{\xi}^2}{2} \delta(\omega - \omega_{\xi}), \quad (5)$$

where $\delta(\omega)$ is the Dirac delta function. The symmetrized correlation function $\mathcal{S}(t)$ and anti-symmetrized correlation function $\mathcal{A}(t)$ of the collective bath coordinate \hat{X} are expressed as

$$\begin{aligned} \mathcal{S}(t) &\equiv \frac{1}{2} \left\langle \left\{ \hat{X}(t), \hat{X}(0) \right\} \right\rangle^{\text{bath}} \\ &= \frac{2}{\pi} \int_0^{\infty} d\omega \mathcal{J}(\omega) \left(n^{\text{BE}}(\omega, T) + \frac{1}{2} \right) \cos \omega t \end{aligned} \quad (6a)$$

and

$$\begin{aligned} \mathcal{A}(t) &\equiv \frac{1}{2i} \left\langle \left[\hat{X}(t), \hat{X}(0) \right] \right\rangle^{\text{bath}} \\ &= -\frac{1}{\pi} \int_0^{\infty} d\omega \mathcal{J}(\omega) \sin \omega t, \end{aligned} \quad (6b)$$

respectively. Here, $[\hat{A}, \hat{B}] \equiv \hat{A}\hat{B} - \hat{B}\hat{A}$, $\{\hat{A}, \hat{B}\} \equiv \hat{A}\hat{B} + \hat{B}\hat{A}$, $\langle \dots \rangle^{\text{bath}} \equiv \text{Tr}^{\text{bath}}\{\dots \hat{\rho}_{\text{eq}}^{\text{bath}}\}$, and $n^{\text{BE}}(\omega, T) = (e^{\beta\hbar\omega} - 1)^{-1}$ is the Bose–Einstein distribution function.

C. Hierarchical equations of motion

To construct the HEOM, we need to express $\mathcal{S}(t)$ and $\mathcal{A}(t)$ as linear combinations of *time basis functions*, $\phi(t) = (\dots, \phi_k(t), \dots)^{\text{T}}$, which satisfy a set of time evolution equations

$$\partial_t \phi(t) = -\gamma \phi(t). \quad (7)$$

Here, the superscripts T on matrices/vectors represent the transposes of the matrices/vectors. When the column vector $\phi(t)$ has K components, $(\gamma)_{jk} = \gamma_{jk}$ is a $K \times K$ matrix. We assume that $\mathcal{S}(t)$ and $\mathcal{A}(t)$ can be evaluated as

$$\mathcal{S}(t) = \sigma^{\text{T}} \mathbf{S} \phi(t) + s_{\delta} \cdot 2\delta(t) \quad (8a)$$

and

$$\mathcal{A}(t) = \sigma^{\text{T}} \mathbf{A} \phi(t), \quad (8b)$$

respectively. Here, s_δ is a real constant, $\boldsymbol{\sigma} = (\dots, \sigma_k, \dots)^T$ is a constant vector common in $\mathcal{S}(t)$ and $\mathcal{A}(t)$, and \mathcal{S} and \mathcal{A} are $K \times K$ matrices, which commute with γ .

Under this parametrization of the bath correlation functions, the time evolution of the reduced density operator $\hat{\rho}(t)$ is rigorously expressed in terms of a set of time differential equations in the HEOM form [21];

$$\begin{aligned} \partial_t \hat{\rho}_{\mathbf{n}}(t) = & -(\mathcal{L} + \hat{\Xi})\hat{\rho}_{\mathbf{n}}(t) - \sum_{j,k} n_j \gamma_{jk} \hat{\rho}_{\mathbf{n}-\mathbf{e}_j+\mathbf{e}_k}(t) \\ & - \sum_k \hat{\Phi}_k \hat{\rho}_{\mathbf{n}+\mathbf{e}_k}(t) - \sum_k n_k \hat{\Theta}_k \hat{\rho}_{\mathbf{n}-\mathbf{e}_k}(t). \end{aligned} \quad (9)$$

Here,

$$\mathcal{L} \equiv -\frac{i}{\hbar} \hat{H}^\times, \quad \hat{\Phi} \equiv \frac{i}{\hbar} \hat{V}^\times, \quad \hat{\Psi} \equiv \frac{1}{\hbar} \hat{V}^\circ \quad (10a)$$

$$\hat{\Phi} = (\dots, \hat{\Phi}_k, \dots) \equiv \boldsymbol{\sigma} \hat{\Phi}, \quad (10b)$$

$$\hat{\Theta} = (\dots, \hat{\Theta}_k, \dots) \equiv \mathcal{S} \phi(0) \hat{\Phi} - \mathcal{A} \phi(0) \hat{\Psi}, \quad (10c)$$

and

$$\hat{\Xi} \equiv -s_\delta \hat{\Phi}^2, \quad (10d)$$

and we have introduced commutation and anti-commutation hyper operators, $\hat{A}^{\times/\circ} \hat{B} \equiv \hat{A} \hat{B} \mp \hat{B} \hat{A}$. The multi-index $\mathbf{n} \equiv (\dots, n_k, \dots)$, whose components are non-negative integers, represents the index of the ‘‘hierarchy,’’ and $\mathbf{e}_k \equiv (0, \dots, 1, 0, \dots)$ is the k th unit vector. The first hierarchical element, $\hat{\rho}_0(t)$, corresponds to the reduced density operator, $\hat{\rho}(t)$, and the rest of the hierarchical elements are introduced in order to facilitate rigorous treatment of the non-Markovian time dependencies of bath correlation functions. Hereafter, we refer to the elements of the hierarchy, $\hat{\rho}_{\mathbf{n}}(t)$, as the auxiliary density operators (ADOs). Under the factorized initial condition Eq. (3), $\hat{\rho}_0(t_0) = \hat{\rho}(t_0)$, and $\hat{\rho}_{\mathbf{n}}(t_0) = 0$ for $\mathbf{n} \neq \mathbf{0}$.

D. ‘‘Basis’’ in hierarchy space

To make the following transformation of the HEOM easier, we introduce a series of functions $\psi_{\mathbf{n}}(\mathbf{x})$, and their raising and lowering operators $\mathbf{h}^+ \equiv (\dots, h_k^+, \dots)^T$ and $\mathbf{h}^- \equiv (\dots, h_k^-, \dots)^T$ as follows:

$$\psi_{\mathbf{0}}(\mathbf{x}) \equiv \frac{1}{\sqrt{\pi |\mathbf{D}|}} \exp\left(-\mathbf{x}^T \frac{1}{\mathbf{D}} \mathbf{x}\right), \quad (11a)$$

$$\psi_{\mathbf{n}}(\mathbf{x}) \equiv \frac{\mathbf{h}^{+\mathbf{n}}}{\mathbf{n}!} \psi_{\mathbf{0}}(\mathbf{x}), \quad (\mathbf{n} \neq \mathbf{0}) \quad (11b)$$

$$\mathbf{h}^+ \equiv -\mathbf{B}^T \sqrt{\frac{\mathbf{D}}{2}} \boldsymbol{\partial}_x, \quad (12a)$$

and

$$\mathbf{h}^- \equiv \mathbf{B}^{-1} \left(\sqrt{\frac{2}{\mathbf{D}}} \mathbf{x} + \sqrt{\frac{\mathbf{D}}{2}} \boldsymbol{\partial}_x \right). \quad (12b)$$

Here, $\mathbf{x} = (\dots, x_k, \dots)^T$ and $\boldsymbol{\partial}_x = (\dots, \partial_{x_k}, \dots)^T$ are a real vector and its differential operator, \mathbf{D} is an arbitrary $K \times K$ real positive-definite matrix, and \mathbf{B} is an arbitrary $K \times K$ real regular matrix. The fraction $1/\mathbf{A}$ denotes the inverse matrix of a matrix \mathbf{A} . We have introduced the following multi-index notation:

$$\begin{aligned} |\mathbf{n}| & \equiv \sum_k n_k, & \mathbf{n}! & \equiv \prod_k n_k!, \\ \boldsymbol{\alpha}^{\mathbf{n}} & \equiv \prod_k \alpha_k^{n_k}, & \delta_{\mathbf{n}, \mathbf{n}'} & \equiv \prod_k \delta_{n_k, n'_k}, \end{aligned} \quad (13)$$

where $\delta_{j,k}$ is the Kronecker delta.

Eqs. (12a) and (12b) satisfy

$$[h_j^+, h_k^-] = -\delta_{j,k} \quad (14a)$$

and

$$h_k^- \psi_{\mathbf{0}}(\mathbf{x}) = 0, \quad (14b)$$

and therefore they have the following raising and lowering relations;

$$h_k^+ \psi_{\mathbf{n}}(\mathbf{x}) = (n_k + 1) \psi_{\mathbf{n}+\mathbf{e}_k}(\mathbf{x}), \quad (15a)$$

and

$$h_k^- \psi_{\mathbf{n}}(\mathbf{x}) = \psi_{\mathbf{n}-\mathbf{e}_k}(\mathbf{x}). \quad (15b)$$

These indicate that $\psi_{\mathbf{n}}(\mathbf{x})$ is pertaining to a multi-dimensional Hermite function. For details, see Appendix A.

It is important that $\psi_{\mathbf{n}}(\mathbf{x})$ has the following orthogonality;

$$\int d\mathbf{x} \psi_{\mathbf{0}}(\mathbf{x})^{-1} \cdot \psi_{\mathbf{n}}(\mathbf{x}) \psi_{\mathbf{n}'}(\mathbf{x}) = \mathbf{n}! \delta_{\mathbf{n}, \mathbf{n}'}. \quad (16)$$

This leads to

$$\int d\mathbf{x} \psi_{\mathbf{n}}(\mathbf{x}) = \begin{cases} 1 & \mathbf{n} = \mathbf{0} \\ 0 & \text{otherwise.} \end{cases} \quad (17)$$

Using $\psi_{\mathbf{n}}(\mathbf{x})$, we introduce the transformation from the set of ADOs $\hat{\rho}_{\mathbf{n}}$ to a function,

$$\tilde{f}(\mathbf{x}, t) \equiv \sum_{\mathbf{n}} \hat{\rho}_{\mathbf{n}}(t) \psi_{\mathbf{n}}(\mathbf{x}), \quad (18a)$$

and its inverse transformation

$$\hat{\rho}_{\mathbf{n}}(t) = \frac{1}{\mathbf{n}!} \int d\mathbf{x} \psi_{\mathbf{0}}(\mathbf{x})^{-1} \cdot \psi_{\mathbf{n}}(\mathbf{x}) \tilde{f}(\mathbf{x}, t). \quad (18b)$$

In other words, we regard the ADOs as linear basis coefficients of $\tilde{f}(\mathbf{x}, t)$. The inverse transformation Eq. (18b) is a generalization of a construction of the so-called Brinkman hierarchy, which is introduced to express momentum degrees of freedom in the Fokker–Planck–Kramers equation [57]. Similar transformations appear in Refs. 17, 44, 45, 48, 52, and 58.

By substituting Eq. (18a) into Eq. (9), we obtain the following time evolution equation:

$$\partial_t \tilde{f}(\mathbf{x}, t) = -\tilde{\mathcal{L}}^f(t) \tilde{f}(\mathbf{x}, t), \quad (19)$$

where

$$\tilde{\mathcal{L}}^f(t) \equiv \mathcal{L}(t) + \hat{\Xi} + \mathbf{h}^{+T} \boldsymbol{\gamma} \mathbf{h}^- + \hat{\Phi}^T \mathbf{h}^- + \mathbf{h}^{+T} \hat{\Theta}. \quad (20)$$

Thus, the discrete degrees of freedom \mathbf{n} in the HEOM are mapped into the continuous degrees of freedom \mathbf{x} . Hereafter, we refer to \mathbf{x} as the auxiliary modes.

E. Mapping into the collective bath coordinate space

The right-hand side of Eq. (19) contains up to the second-order differential operator of \mathbf{x} , and Eq. (17) makes $\tilde{f}(\mathbf{x}, t)$ satisfy

$$\int d\mathbf{x} \tilde{f}(\mathbf{x}, t) = \hat{\rho}_0(t) = \hat{\rho}(t). \quad (21)$$

Thus, $\tilde{f}(\mathbf{x}, t)$ acts like a quasi-distribution and Eq. (19) can be regarded as a type of generalization of the quantum Fokker–Planck equation [18, 30, 45, 49–52]. However, $\phi(t)$ usually contains components caused by the Bose–Einstein distribution $n^{\text{BE}}(\omega)$, which are essentially different from the components caused by the spectral density $\mathcal{J}(\omega)$: the latter has mechanical origin while the former does not have. In Eq. (19), both components are coupled to quantum states of the system through $\hat{\Phi}$ and $\hat{\Theta}$, and this makes difficult to interpret the physical meanings of quasi-distribution $\tilde{f}(\mathbf{x}, t)$. In the following, we introduce a transformation of $\tilde{f}(\mathbf{x}, t)$ which clearly separates these two different types of degrees of freedom.

1. Drude spectral density

Hereafter, we assume that a Drude spectral density,

$$\mathcal{J}^{\text{D}}(\omega) \equiv 2\eta \frac{\gamma^{\text{D}} \omega}{\omega^2 + \gamma^{\text{D}2}}, \quad (22)$$

which is dealt with in the original HEOM [17]. We employ the following decomposition of the Bose–Einstein distribution:

$$n^{\text{BE}}(\omega) + \frac{1}{2} = \frac{1}{\beta \hbar \omega} + \sum_{\xi} \frac{2\alpha^{(\xi)}}{\beta \hbar \nu^{(\xi)}} \frac{\omega \nu^{(\xi)2m^{(\xi)} - 1}}{(\omega^2 + \nu^{(\xi)2})^{m^{(\xi)}}} + \Delta \beta \hbar \omega. \quad (23)$$

This form unifies the Pade spectral decomposition (PSD) and Fano spectral decomposition (FSD) schemes [35, 59, 60]. To obtain $\mathcal{S}(t)$ and $\mathcal{A}(t)$, we need to evaluate integrals over poles on $\omega = \pm \nu^{(\xi)}$. In the previous works, the higher-order poles for $m^{(\xi)} > 1$ are evaluated using the

residue theorem, which causes complicated expressions for coefficients and difficulties in analytical transformations [21, 36]. In Appendix B, we introduce a new evaluation theorem of the higher-order residues using matrix forms, and the results in the present case of the Drude spectral density are

$$\mathcal{S}(t) = \sigma^{\text{D}} S^{\text{D}} \phi^{\text{D}}(t) + \sum_{\xi} \sigma^{\text{BE}(\xi)T} \mathbf{S}^{\text{BE}(\xi)} \phi^{\text{BE}(\xi)}(t) + s_{\delta} \cdot 2\delta(t) \quad (24a)$$

and

$$\mathcal{A}(t) = \sigma^{\text{D}} A^{\text{D}} \phi^{\text{D}}(t) \quad (24b)$$

for $t \geq 0$, where

$$\phi^{\text{D}}(t) \equiv \gamma_{\text{D}} e^{-\gamma_{\text{D}} t}, \quad (25a)$$

$$S^{\text{D}} \equiv -2\text{Im} \left\{ \eta \left(n_{\text{BE}}(i\gamma^{\text{D}}) + \frac{1}{2} \right) \right\}, \quad (25b)$$

$$A^{\text{D}} \equiv -\eta, \quad (25c)$$

$$\sigma^{\text{D}} \equiv 1, \quad (25d)$$

$$\phi^{\text{BE}(\xi)}(t) \equiv \tilde{\nu}^{(\xi)} e^{-\tilde{\nu}^{(\xi)} t} \mathbf{e}_1^{(\xi)}, \quad (26a)$$

$$\mathbf{S}^{\text{BE}(\xi)} \equiv -2\text{Im} \left\{ \mathcal{J}^{\text{D}}(i\tilde{\nu}^{(\xi)}) \frac{2\alpha^{(\xi)}}{\beta \hbar \nu^{(\xi)}} \frac{\nu^{(\xi)m^{(\xi)}}}{(\tilde{\nu}^{(\xi)} + \nu^{(\xi)})^{m^{(\xi)}}} \right\}, \quad (26b)$$

$$\sigma^{\text{BE}(\xi)} \equiv \mathbf{e}_{m_{\xi}}^{(\xi)}, \quad (26c)$$

and

$$s_{\delta} \equiv 2\eta \Delta \beta \hbar \gamma_{\text{D}}. \quad (27)$$

Here, $\tilde{\nu}^{(\xi)}$ is a $m^{(\xi)} \times m^{(\xi)}$ matrix defined as

$$\tilde{\nu}^{(\xi)} \equiv \nu^{(\xi)} \begin{pmatrix} 1 & 0 & \dots & 0 \\ -1 & 1 & 0 & \ddots \\ 0 & \ddots & \ddots & 0 \\ \vdots & \ddots & \ddots & 1 \\ 0 & \dots & 0 & -1 \end{pmatrix}, \quad (28a)$$

i.e.,

$$\left(\tilde{\nu}^{(\xi)} \right)_{jk} = \nu^{(\xi)} (\delta_{j,k} - \delta_{j,k+1}). \quad (28b)$$

The $m^{(\xi)}$ -vector $\mathbf{e}_k^{(\xi)}$ is the k th unit vector ($1 \leq k \leq m^{(\xi)}$). The sum between a matrix \mathbf{A} and a scalar B , $\mathbf{A} + B$, indicates $\mathbf{A} + B\mathbf{1}$, where $\mathbf{1}$ is the identity matrix with the same size as \mathbf{A} . In the above expressions, $\phi^{\text{D}}(t)$ describes the component from the Drude spectral density, and $\phi^{\text{BE}(\xi)}(t)$ represents the component from the ξ th pole of Eq. (23). Obviously, $\phi^{\text{BE}(\xi)}(t)$ satisfies $\partial_t \phi^{\text{BE}(\xi)}(t) = -\tilde{\nu}^{(\xi)} \phi^{\text{BE}(\xi)}(t)$, and $\mathbf{s}^{\text{BE}(\xi)}$ commutes with $\tilde{\nu}^{(\xi)}$, and therefore the block-diagonalized expressions,

$$\gamma = \begin{pmatrix} \gamma^D & & & \mathbf{0} \\ & \ddots & & \\ & & \tilde{\nu}^{\text{BE}(\xi)} & \\ \mathbf{0} & & & \ddots \end{pmatrix}, \quad \phi(t) = \begin{pmatrix} \phi^D(t) \\ \vdots \\ \phi^{\text{BE}(\xi)}(t) \\ \vdots \end{pmatrix}, \quad \sigma = \begin{pmatrix} \sigma^D \\ \vdots \\ \sigma^{\text{BE}(\xi)} \\ \vdots \end{pmatrix}, \quad (29a)$$

$$\mathbf{S} = \begin{pmatrix} S^D & & & \mathbf{0} \\ & \ddots & & \\ & & \mathbf{S}^{\text{BE}(\xi)} & \\ \mathbf{0} & & & \ddots \end{pmatrix}, \quad \text{and} \quad \mathbf{A} = \begin{pmatrix} A^D & & & \mathbf{0} \\ & \ddots & & \\ & & \mathbf{0} & \\ \mathbf{0} & & & \ddots \end{pmatrix}, \quad (29b)$$

satisfy the required conditions to construct the HEOM theory.

The corresponding Eqs.(9) and (19) are

$$\begin{aligned} \partial_t \hat{\rho}_{n^D, \mathbf{n}^{\text{BE}}}(t) &= - \left(\mathcal{L}(t) + \hat{\Xi} \right) \hat{\rho}_{n^D, \mathbf{n}^{\text{BE}}}(t) \\ &\quad - n^D \gamma^D \hat{\rho}_{n^D, \mathbf{n}^{\text{BE}}}(t) \\ &\quad - \hat{\Phi} \rho_{n^D+1, \mathbf{n}^{\text{BE}}}(t) - n^D \hat{\Theta}^D \rho_{n^D-1, \mathbf{n}^{\text{BE}}}(t) \\ &\quad - \sum_{\xi} \sum_{j,k} n_j^{\text{BE}(\xi)} \tilde{\nu}_{jk}^{(\xi)} \hat{\rho}_{n^D, \mathbf{n}^{\text{BE}} - \mathbf{e}_j^{(\xi)} + \mathbf{e}_k^{(\xi)}}(t) \\ &\quad - \sum_{\xi} \sum_k \hat{\Phi} \sigma_k^{\text{BE}(\xi)} \hat{\rho}_{n^D, \mathbf{n}^{\text{BE}} + \mathbf{e}_k^{(\xi)}}(t) - \sum_{\xi} \sum_j n_j^{\text{BE}(\xi)} \hat{\Theta}_j^{\text{BE}(\xi)} \hat{\rho}_{n^D, \mathbf{n}^{\text{BE}} - \mathbf{e}_j^{(\xi)}}(t) \end{aligned} \quad (30)$$

and

$$\partial_t \tilde{f}(x^D, \mathbf{x}^{\text{BE}}, t) = -\tilde{\mathcal{L}}^f(t) \tilde{f}(x^D, \mathbf{x}^{\text{BE}}, t), \quad (31)$$

where

$$\begin{aligned} \tilde{\mathcal{L}}^f(t) &\equiv \mathcal{L}(t) + \hat{\Xi} + h^{D+} \gamma^D h^{D-} + \hat{\Phi} h^{D-} + h^{D+} \hat{\Theta}^D \\ &\quad + \sum_{\xi} \left(\mathbf{h}^{\text{BE}(\xi)+T} \tilde{\nu}^{(\xi)} \mathbf{h}^{\text{BE}(\xi)-} + \hat{\Phi} \sigma^{\text{BE}(\xi)T} \mathbf{h}^{\text{BE}(\xi)-} + \mathbf{h}^{\text{BE}(\xi)+T} \hat{\Theta}^{\text{BE}(\xi)} \right) \end{aligned} \quad (32)$$

Here, we have introduced the hierarchy multi-index $\mathbf{n} = (n^D, \mathbf{n}^{\text{BE}})$, the corresponding continuous degrees of freedom, $\mathbf{x} = (x^D, \mathbf{x}^{\text{BE}})$, and the raising/lowering operators, $\mathbf{h}^{\pm} = (h^{D\pm}, \mathbf{h}^{\text{BE}\pm})$. The multi-index/vector for the components from the Bose–Einstein distribution consists of the set of sub-multi-indices/vectors for the ξ th pole, e.g., $\mathbf{n}^{\text{BE}} = (\dots, \mathbf{n}^{\text{BE}(\xi)}, \dots)$, and $\mathbf{n}^{\text{BE}(\xi)}$ is $m^{(\xi)}$ -dimensional multi-index, e.g., $\mathbf{n}^{\text{BE}(\xi)} = (n_0^{\text{BE}(\xi)}, \dots, n_{m^{(\xi)}}^{\text{BE}(\xi)})$. The summations of j and k run over $j, k = 1, \dots, \leq m^{(\xi)}$. Thus, \mathbf{n}^{BE} has K^{BE} dimension, where $K^{\text{BE}} \equiv \sum_{\xi} m^{(\xi)}$.

The operators appearing in these expressions are defined as

$$\hat{\Theta}^D \equiv S^D \phi^D(0) \hat{\Phi} - A^D \phi^D(0) \hat{\Psi}, \quad (33a)$$

$$\hat{\Theta}^{\text{BE}(\xi)} \equiv \mathbf{S}^{\text{BE}(\xi)} \phi^{\text{BE}(\xi)}(0) \hat{\Phi}, \quad (33b)$$

and

$$\hat{\Xi} \equiv -s_{\delta} \hat{\Phi}^2. \quad (33c)$$

2. Mixing and renormalizing of “the hierarchy space”

As mentioned above, the auxiliary modes $\mathbf{x}^{\text{BE}(\xi)}$ come from Eq. (23) are coupled to system states through operators $\hat{\Phi} \mathbf{h}^{\text{BE}(\xi)\pm}$, which makes difficult to interpret the roles of x^D and \mathbf{x}^{BE} . Here, we consider the following transformation:

$$\hat{f}(x^D, \mathbf{x}^{\text{BE}}, t) \equiv \mathcal{S}^{\text{ren}} \mathcal{S}^{\text{mix}} \tilde{f}(x^D, \mathbf{x}^{\text{BE}}, t), \quad (34)$$

where

$$\mathcal{S}^{\text{mix}} \equiv \exp \left[\frac{a^D}{2} (h^{D+})^2 + \sum_{\xi} \left(\mathbf{h}^{\text{BE}(\xi)+T} \mathbf{a}^{\text{BE}(\xi)+} + \mathbf{a}^{\text{BE}(\xi)-T} \mathbf{h}^{\text{BE}(\xi)-} \right) h^{D+} \right] \quad (35)$$

and

$$\mathcal{S}^{\text{ren}} \equiv \exp \left[\sum_{\xi} \mathbf{h}^{\text{BE}(\xi)+\text{T}} \ln \left(-\mathbf{C}^{\text{BE}(\xi)} \right) \mathbf{h}^{\text{BE}(\xi)-} \right]. \quad (36)$$

Here, a^{D} is a constant, $\mathbf{a}^{\text{BE}(\xi)\pm}$ are $(m^{(\xi)}+1)$ -dimensional vectors, and $\mathbf{C}^{\text{BE}(\xi)}$ is a $m^{(\xi)} \times m^{(\xi)}$ regular matrix. The transformation by Eq. (35) causes mixing of modes x^{D} and \mathbf{x}^{BE} in hierarchy spaces:

$$\left\{ \begin{array}{l} \mathcal{S}^{\text{mix}} h^{\text{D}+} \mathcal{S}^{\text{mix}-1} = h^{\text{D}+}, \\ \mathcal{S}^{\text{mix}} h^{\text{D}-} \mathcal{S}^{\text{mix}-1} = h^{\text{D}-} - \sum_{\xi} \left(\mathbf{h}^{\text{BE}(\xi)+\text{T}} \mathbf{a}^{\text{BE}(\xi)+} + \mathbf{a}^{\text{BE}(\xi)-\text{T}} \mathbf{h}^{\text{BE}(\xi)-} \right) - a^{\text{D}} h^{\text{D}+}, \\ \mathcal{S}^{\text{mix}} \mathbf{h}^{\text{BE}(\xi)+\text{T}} \mathcal{S}^{\text{mix}-1} = \mathbf{h}^{\text{BE}(\xi)+\text{T}} + \mathbf{a}^{\text{BE}(\xi)-\text{T}} h^{\text{D}+}, \\ \mathcal{S}^{\text{mix}} \mathbf{h}^{\text{BE}(\xi)-} \mathcal{S}^{\text{mix}-1} = \mathbf{h}^{\text{BE}(\xi)-} - \mathbf{a}^{\text{BE}(\xi)+} h^{\text{D}+}. \end{array} \right. \quad (37)$$

On the other hand, the transformation by Eq. (36) causes renormalization of raising/lowering relation in \mathbf{x}^{BE} :

$$\left\{ \begin{array}{l} \mathcal{S}^{\text{ren}} \mathbf{h}^{\text{BE}(\xi)+\text{T}} \mathcal{S}^{\text{ren}-1} = \mathbf{h}^{\text{BE}(\xi)+\text{T}} \mathbf{C}^{\text{BE}(\xi)}, \\ \mathcal{S}^{\text{ren}} \mathbf{h}^{\text{BE}(\xi)-} \mathcal{S}^{\text{ren}-1} = \mathbf{C}^{\text{BE}(\xi)-1} \mathbf{h}^{\text{BE}(\xi)-}. \end{array} \right. \quad (38)$$

Under this transformation, time evolution of $\hat{f}(x^{\text{D}}, \mathbf{x}^{\text{BE}}, t)$ can be evaluated as

$$\partial_t \hat{f}(x^{\text{D}}, \mathbf{x}^{\text{BE}}, t) = -\hat{\mathcal{L}}^f(t) \hat{f}(x^{\text{D}}, \mathbf{x}^{\text{BE}}, t), \quad (39)$$

where

$$\hat{\mathcal{L}}^f(t) \equiv \mathcal{S}^{\text{ren}} \mathcal{S}^{\text{mix}} \tilde{\mathcal{L}}^f(t) \mathcal{S}^{\text{ren}-1} \mathcal{S}^{\text{mix}-1}. \quad (40)$$

We choose the parameters of these transformations as

$$\mathbf{a}^{\text{BE}(\xi)+} = \mathbf{s}^{\text{BE}(\xi)} \phi^{\text{BE}(\xi)}(0), \quad (41a)$$

$$\mathbf{a}^{\text{BE}(\xi)-} = \boldsymbol{\sigma}^{\text{BE}(\xi)}, \quad (41b)$$

$$a^{\text{D}} = -\frac{1}{\gamma^{\text{D}}} \sum_{\xi} \boldsymbol{\sigma}^{\text{BE}(\xi)\text{T}} \tilde{\boldsymbol{\nu}}^{(\xi)} \mathbf{s}^{\text{BE}(\xi)} \phi^{\text{BE}(\xi)}(0), \quad (41c)$$

and

$$\mathbf{C}^{\text{BE}(\xi)} = (\gamma^{\text{D}} - \tilde{\boldsymbol{\nu}}^{(\xi)}) / \tilde{g}. \quad (42)$$

Here, \tilde{g} is a scaling constant of which value is determined later. Then, all the terms including $\hat{\Phi} \mathbf{h}^{\text{BE}(\xi)\pm}$ in Eq. (32) cancel, and we obtain

$$\begin{aligned} \hat{\mathcal{L}}^f(t) = & \mathcal{L}(t) + \hat{\Xi} + h^{\text{D}+} \gamma^{\text{D}} h^{\text{D}-} + \hat{\Phi} h^{\text{D}-} + h^{\text{D}+} \left(S'^{\text{D}} \hat{\Phi} - A'^{\text{D}} \hat{\Psi} \right) \\ & + \sum_{\xi} \left(\mathbf{h}^{\text{BE}(\xi)+\text{T}} \tilde{\boldsymbol{\nu}}^{(\xi)} \mathbf{h}^{\text{BE}(\xi)-} \right. \\ & \left. + h^{\text{D}+} \mathbf{h}^{\text{BE}(\xi)+\text{T}} \mathbf{S}'^{\text{BE}(\xi)} \phi^{\text{BE}(\xi)}(0) - h^{\text{D}+} \boldsymbol{\sigma}'^{\text{BE}(\xi)\text{T}} \mathbf{h}^{\text{BE}(\xi)-} \right). \end{aligned} \quad (43)$$

Here,

$$\mathbf{S}'^{\text{BE}(\xi)} \equiv (\tilde{\boldsymbol{\nu}}^{(\xi)2} - \gamma^{\text{D}2}) \mathbf{S}^{\text{BE}(\xi)} / \tilde{g}, \quad (44b)$$

$$S'^{\text{D}} \equiv 2\eta \left(\frac{1}{\beta \hbar} + \sum_{\xi} \frac{2\alpha^{(\xi)}}{\beta \hbar} \delta_{1,m^{(\xi)}} - \Delta \beta \hbar \gamma^{\text{D}2} \right), \quad (44a)$$

$$\boldsymbol{\sigma}'^{\text{BE}(\xi)} \equiv \tilde{g} \boldsymbol{\sigma}^{\text{BE}(\xi)}, \quad (44c)$$

and

$$A'^D \equiv -\eta\gamma_D. \quad (44d)$$

In Eq. (43), only x^D couples to the quantum states of the system through $\hat{\Phi}$ and $\hat{\Psi}$. This indicates that x^D is proportional to the collective bath coordinate X . Note that, the transformations Eqs. (35) and (36) do not change the value of integral,

$$\begin{aligned} & \int dx^D \int d\mathbf{x}^{\text{BE}} \hat{f}(x^D, \mathbf{x}^{\text{BE}}, t) \\ &= \int dx^D \int d\mathbf{x}^{\text{BE}} \tilde{f}(x^D, \mathbf{x}^{\text{BE}}, t) \\ &= \hat{\rho}_0(t) = \hat{\rho}(t). \end{aligned} \quad (45)$$

F. Partial and full quantum Fokker–Planck representation

In order to see the role of the mode x^D clearly, we set parameters of basis $\psi_{\mathbf{n}}(\mathbf{x})$ as follows:

$$D = \begin{pmatrix} D^D & \mathbf{0} \\ \mathbf{0} & D^{\text{BE}} \end{pmatrix} \quad (46a)$$

and

$$B = \begin{pmatrix} B^D & \mathbf{0} \\ \mathbf{0} & B^{\text{BE}} \end{pmatrix}. \quad (46b)$$

This leads

$$h^{D+} = -B^D \sqrt{\frac{D^D}{2}} \partial_x \quad (47a)$$

and

$$h^{D-} = +\frac{1}{B^D} \left(\sqrt{\frac{2}{D^D}} \mathbf{x} + \sqrt{\frac{D^D}{2}} \partial_x \right). \quad (47b)$$

By setting

$$D^D = \frac{2}{\omega^f} \left(\frac{1}{\beta\hbar} + \sum_{\xi} \frac{2\alpha^{(\xi)}}{\beta\hbar} \delta_{1,m^{(\xi)}} - \Delta\beta\hbar\gamma_D^2 \right) \quad (48a)$$

and

$$B^D = -\frac{1}{\sqrt{D^D\eta\omega^f}} \quad (48b)$$

with an arbitrary positive scaling constant ω^f , we obtain

$$\begin{aligned} \hat{\mathcal{L}}^f(t) &= \frac{i}{\hbar} \hat{H}^f(t)^\times + r^f \partial_q \left(-\frac{1}{2\hbar} \left(\partial_q \hat{H}^f(t) \right)^\circ \right) + \hat{\Xi} - \left(s_\delta^f + s_\Delta^{f\text{BE}} \right) \partial_q^2 \\ &+ \sum_{\xi} \mathbf{h}^{\text{BE}(\xi)+\text{T}} \tilde{\nu}^{(\xi)} \mathbf{h}^{\text{BE}(\xi)-} + \partial_q \sum_{\xi} \mathbf{h}^{\text{BE}(\xi)+\text{T}} \mathbf{s}^{f\text{BE}(\xi)} - \partial_q \sum_{\xi} \boldsymbol{\sigma}^{\text{BE}(\xi)\text{T}} \mathbf{h}^{\text{BE}(\xi)-} \end{aligned} \quad (49)$$

Here, we rewrite x^D as q ,

$$\hat{H}^f(t) \equiv \hat{H}(t) - \hbar g^f \hat{V} q + \frac{\hbar\omega^f}{2} q^2, \quad (50)$$

$$g^f \equiv -\frac{1}{B^D} \sqrt{\frac{2}{D^D}} = \sqrt{2\eta\omega^f}, \quad (51)$$

$$r^f \equiv \frac{\gamma^D}{\omega^f}, \quad (52a)$$

$$s^f \equiv \frac{\gamma^D}{\beta\hbar\omega^f} \left(1 + \sum_{\xi} 2\alpha^{(\xi)} \delta_{1,m^{(\xi)}} \right), \quad (52b)$$

$$\mathbf{s}^{f\text{BE}(\xi)} \equiv \mathbf{S}^{f\text{BE}(\xi)} \boldsymbol{\phi}^{\text{BE}(\xi)}(0), \quad (52c)$$

$$\mathbf{S}^{f\text{BE}(\xi)} \equiv \frac{\gamma^D}{\omega^f} \frac{2\alpha^{(\xi)}}{\beta\hbar\nu^{(\xi)}} \frac{2\tilde{\nu}^{(\xi)} \nu^{(\kappa) m^{(\kappa)}}}{(\tilde{\nu}^{(\xi)} + \nu^{(\xi)})^{m^{(\xi)}}}, \quad (52d)$$

$$s_\Delta^{f\text{BE}} \equiv -\frac{\gamma^D}{\omega^f} \Delta\beta\hbar\gamma_D^2, \quad (52e)$$

and set $\tilde{g} = g^f$. It is remarkable that, in Eq. (49), the coupling between the system and q is described by, and only by, an extended Hamiltonian Eq. (50). Eqs. (2b) and (50) leads $X = g^f q$, and hence $\hat{f}(q, \mathbf{x}^{\text{BE}}, t)$ is a joint distribution between system space, collective bath coordinate space, and auxiliary modes \mathbf{x}^{BE} . It is notable that q entirely describes the non-Markovian part of the system-bath interaction, the Markovian part caused by the last term of Eq. (24a) is described by $\hat{\Xi}$. It is also important that, the coupling strength constant η appears only in Eq. (50) through g^f , and hence the constant does not affect the connection between q and \mathbf{x}^{BE} .

Note that the construction of a joint distribution between system space and collective bath coordinate space has been given by Shi and co-workers in Ref. 47. Our transformation Eq. (34) can be regarded an extension of their work, with its time evolution equation Eq. (49). For details, see Appendix C.

Eq. (34) can be regarded as a special case of inverse of the transformation of spectral densities given by Legget

[43, 61]. Variants of the transformation are used in the so-called reaction coordinate mapping approaches, which are another series of an open quantum theory that describes non-Markovian non-perturbative system-environment coupling effects [14, 62, 63]. In our work, a similar mapping is performed in hierarchical space instead of in spectral density functions.

By applying Eq. (18b) partially,

$$\hat{f}_{\mathbf{n}^{\text{BE}}}(q, t) = \frac{1}{\mathbf{n}^{\text{BE}}!} \int d\mathbf{x}^{\text{BE}} \psi_{\mathbf{0}}^{\text{BE}}(\mathbf{x}^{\text{BE}})^{-1} \times \psi_{\mathbf{n}^{\text{BE}}}(\mathbf{x}^{\text{BE}}) \hat{f}(q, \mathbf{x}^{\text{BE}}, t), \quad (53)$$

we obtain the partial hierarchical representation (or the partial quantum Fokker–Planck representation) of Eq. (49) as

$$\begin{aligned} \partial_t \hat{f}_{\mathbf{n}}(q, t) = & - \left[\frac{i}{\hbar} \hat{H}^{\text{ext}}(t)^\times + \Xi \right] \hat{f}_{\mathbf{n}}(q, t) \\ & - r^f \partial_q \left(-\frac{1}{2\hbar} \partial_q \hat{H}^{\text{ext}}(t)^\circ \right) \hat{f}_{\mathbf{n}}(q, t) \\ & + \left(s^f + s_{\Delta}^{\text{fBE}} \right) \partial_q^2 \hat{f}_{\mathbf{n}}(q, t) \\ & - \sum_{\xi} \sum_{j,k} \tilde{\nu}_{jk}^{(\xi)} n_j^{(\xi)} \hat{f}_{\mathbf{n}-\mathbf{e}_j^{(\xi)} + \mathbf{e}_k^{(\xi)}}(q, t) \\ & - \sum_{\xi} \sum_j \partial_q s_j^{\text{fBE}(\xi)} n_j^{(\xi)} \hat{f}_{\mathbf{n}-\mathbf{e}_j^{(\xi)}}(q, t) \\ & + \sum_{\xi} \sum_j \partial_q \sigma_j^{\text{BE}(\xi)} \hat{f}_{\mathbf{n}+\mathbf{e}_j^{(k)}}(q, t). \end{aligned} \quad (54)$$

Clearly, this is an extension of the multi-state low-temperature quantum Smoluchowski equation (MS-LT-QSE) we derived in the previous works [45, 64]; If the Markovian part comes from Eq. (23) does not exist (i.e. $\Delta = 0$) and we use only poles of order 1 (i.e. $m^{(\xi)} = 1$), Eq. (54) reduces the MS-LT-QSE.

It is also possible to construct a definite full quantum Fokker–Planck representation by setting values of matrices \mathbf{D}^{BE} and \mathbf{B}^{BE} . We found that the following choice causes a simple equation; We employ the following block diagonalized form,

$$\mathbf{D}^{\text{BE}} = \begin{pmatrix} \ddots & & \mathbf{0} \\ & \mathbf{D}^{\text{BE}(\xi)} & \\ \mathbf{0} & & \ddots \end{pmatrix} \quad (55a)$$

and

$$\mathbf{B}^{\text{BE}} = \begin{pmatrix} \ddots & & \mathbf{0} \\ & \mathbf{B}^{\text{BE}(\xi)} & \\ \mathbf{0} & & \ddots \end{pmatrix}. \quad (55b)$$

We set $\mathbf{D}^{\text{BE}(\xi)}$ as the Lyapunov solution of the following continuous Lyapunov equation [65],

$$\frac{1}{4} \tilde{\nu}^{(\xi)} \mathbf{D}^{\text{BE}(\xi)} + \mathbf{D}^{\text{BE}(\xi)} \frac{1}{4} \tilde{\nu}^{(\xi)\text{T}} = \Sigma^{\text{BE}(\xi)}, \quad (56)$$

and choose $\mathbf{B}^{\text{BE}(\xi)}$ as

$$\mathbf{B}^{\text{BE}(\xi)} = -\sqrt{\frac{2\omega^{\text{D}}}{\gamma^{\text{D}}}} \mathbf{D}^{\text{BE}(\xi)-1/2} \tilde{\nu}^{(\xi)-1}. \quad (57)$$

Then we obtain,

$$\begin{aligned} \hat{\mathcal{L}}^f(t) \equiv & \frac{i}{\hbar} \hat{H}^{\text{ext}}(t)^\times + r^f \left(-\partial_q \frac{1}{2\hbar} \hat{H}^{\text{ext}}(t)^\circ \right) \\ & + \hat{\Xi} - \partial_q \left(s^f + s_{\Delta}^{\text{fBE}} \right) \partial_q^2 \\ & - \sum_{\xi} \partial_x^{\text{BE}(\xi)\text{T}} \left(\tilde{\nu}^{(\xi)} \mathbf{x}^{\text{BE}(\xi)} + \Sigma^{\text{BE}(\xi)} \partial_x^{\text{BE}(\xi)} \right) \\ & + g^{\text{BE}} \sum_{\xi} \partial_q \sigma^{\text{BE}(\xi)\text{T}} \left(\tilde{\nu}^{(\xi)} \mathbf{x}^{\text{BE}(\xi)} + 2\Sigma^{\text{BE}(\xi)} \partial_x^{\text{BE}(\xi)} \right). \end{aligned} \quad (58)$$

Here,

$$g^{\text{BE}} \equiv \sqrt{r^f} \quad (59)$$

and

$$\Sigma^{\text{BE}(\xi)} \equiv \frac{2\alpha^{(\xi)}}{\beta\hbar} \mathbf{e}_1 \mathbf{e}_1^{\text{T}}. \quad (60)$$

G. The factorized initial condition

As explained in Sec. II C, in the case of the factorized initial condition, Eq. (3), only the first hierarchy has a non-zero value, $\hat{\rho}_{\mathbf{0}}(t_0) = \hat{\rho}(t_0)$. Hence, the corresponding $\hat{f}(q, \mathbf{x}^{\text{BE}}, t_0)$ is

$$\hat{f}(q, \mathbf{x}^{\text{BE}}, t_0) = \mathcal{S}^{\text{ren}} \mathcal{S}^{\text{mix}} \hat{\rho}(t_0) \psi_{\mathbf{n}}(q, \mathbf{x}^{\text{BE}}). \quad (61)$$

In the case of the partial hierarchical representation Eq. (54), this expression causes the following recurrence relations at $t = t_0$.

$$\hat{f}_{\mathbf{0}}(q, t_0) = \frac{1}{\sqrt{2\pi D_{[\gamma^{\text{D}}]}^{\text{fBE}}}} \exp\left(-\frac{q^2}{2D^{\text{fBE}}}\right) \quad (62a)$$

$$\hat{f}_{\mathbf{n}+\mathbf{e}_k^{(\xi)}}(q, t_0) = -s_{[\gamma^{\text{D}}]k}^{\text{fBE}(\xi)} \partial_q \hat{f}_{\mathbf{n}}(q, t_0) \quad (62b)$$

and

$$\left(q + \frac{D_{[\gamma^{\text{D}}]}^{\text{fBE}}}{4} \partial_q \right) \hat{f}_{\mathbf{n}}(q, t_0) = \sum_{\xi} \sum_k s_{[\gamma^{\text{D}}]k}^{\text{fBE}(\xi)} n_k^{\text{BE}(\xi)} \hat{f}_{\mathbf{n}-\mathbf{e}_k^{(\xi)}}(q, t_0), \quad (62c)$$

where

$$s_{[\gamma^{\text{D}}]}^{\text{fBE}(\xi)} \equiv \frac{1}{\tilde{\nu}^{(\xi)} + \gamma^{\text{D}}} s^{\text{fBE}(\xi)} \quad (63)$$

and

$$D_{[\gamma^D]}^{f\text{BE}} \equiv \frac{1}{\gamma^D} \left(s^f + s_{\Delta}^{f\text{BE}} - \sum_{\xi} \sigma^{\text{BE}(\xi)\text{T}} s_{[\gamma^D]}^{f\text{BE}(\xi)} \right). \quad (64)$$

By substituting Eqs. (62a)–(62c), it is shown that the right-hand-side of Eq. (54) becomes zero when $\eta = 0$ and $H \times \hat{\rho}(t_0) = 0$. Thus, Eqs. (62a)–(62c) represents the thermal equilibrium state of the bath uncoupled to the system.

Note that, while $D_{[\gamma^D]}^{f\text{BE}}$ corresponds to the variance of the corrective coordinate q uncoupled to the system, this value diverges when we increase the number of poles of order 1 in the Bose–Einstein distribution decomposition Eq. (23). In the case of the exact Matsubara decomposition with an infinity number of poles,

$$n^{\text{BE}}(\omega) + \frac{1}{2} = \frac{1}{\beta\hbar\omega} + \sum_{\xi=1}^{\infty} \frac{2}{\beta\hbar} \frac{\omega}{\omega^2 + \nu^{\text{M}(\xi)2}}, \quad (65)$$

we obtain

$$D_{[\gamma^D]}^{f\text{BE}} = \sum_{\xi=-\infty}^{\infty} \frac{1}{\beta\hbar\omega^f} \frac{\gamma^D}{|\nu^{\text{M}(\xi)}| + \gamma^D} \rightarrow \infty. \quad (66)$$

Here, $\nu^{\text{M}(\xi)} = 2\pi\xi/\beta\hbar$ is the ξ th Matsubara frequency. Hence, we may not discuss the value of $\hat{f}(q, \mathbf{x}^{\text{BE}}, t)$ in a quantitative manner. However, this gives the exact evaluation of the reduced operator through Eq. (45); High-frequency components $\nu^{(\xi)} \gg 1$ do not couple to quantum states of the system because of the difference of time scales. This divergence is a result of the Drude spectral density model Eq. (22), which causes $\mathcal{S}(0) \rightarrow \infty$, and essentially comes from the ultraviolet divergence of the corresponding Ohmic spectral density (See Ref. 45).

While the values of $\hat{f}(q, \mathbf{x}^{\text{BE}}, t)$ may be interpreted quantitatively, qualitative consideration about the values could be useful because they are parts of the exact description of the effect of system-bath interaction.

H. Truncation of hierarchy

Because the full and partial hierarchical forms, Eqs. (30) and (54), consist of sets of infinitely many differential equations, we need to truncate \mathbf{n} in order to carry out numerical calculations. In the case of the ordinary HEOM Eq. (30), we usually take a subset which consists of a definite number of hierarchy elements into numerical calculations, $\mathbf{n} \in \{\mathcal{N}\}$, and we regard the rest elements as $\hat{\rho}_{\mathbf{n}}(t) = 0$ ($\mathbf{n} \notin \{\mathcal{N}\}$). This treatment implies that, we assume that the values of the deep hierarchy elements are unchanged from those in the factorized initial condition, Eq. (3). In the case of Eq. (54), the hierarchy elements $\hat{f}_{\mathbf{n}}(q, t)$ have non-zero values under the factorized

initial condition. Therefore, we need a different strategy; In this paper, we take a subset of $\hat{f}_{\mathbf{n}}(q, t)$ ($\mathbf{n} \in \{\mathcal{N}\}$) into the numerical calculations, and assume that the rest elements can be evaluated using the recurrence relation under the factorized initial condition, Eq. (62b). It is crucial to validate these truncation schemes by changing the size of the subset to obtain numerically exact results.

The choice of subset $\{\mathcal{N}\}$ affects the efficiency of calculations, and many advanced methods are proposed within the HEOM framework [47, 66–68]. In this paper, in order to make the validation of theories simple, we choose the subset in accordance with the condition that \mathbf{n} satisfies $|\mathbf{n}| \equiv \mathcal{N} \leq \mathcal{N}^{\text{max}}$ [34, 38]. This choice is one of the most reliable methods as of now; Most of the other methods are introduced in order to decrease the number of elements for numerical efficiency, and it could sometimes be unstable. Hereafter, we refer to \mathcal{N}^{max} as the depth of the hierarchy, and to the number of elements of the subsets as the size of the hierarchy.

III. NUMERICAL RESULTS

As we explained in the previous section, to perform calculations based on equations that have hierarchical forms, we need to treat a finite number of elements numerically. Generally, the stronger the system-bath coupling becomes, the larger subset we need. In this section, we show that the size of the subset which is required by the ordinary HEOM, Eq. (30), increases rapidly as the coupling strength increases, and it becomes difficult to handle numerically. In contrast, while Eq. (54) requires relatively large computational resources to treat continuous degrees of freedom q , it is possible to handle strong coupling cases in which the HEOM becomes nearly unsolvable.

Hereafter, we employ the dimensionless units $\hbar = 1$ and $k_{\text{B}} = 1$ for simplicity. In order to avoid numerical instabilities caused by time integration schemes, we employ the Dormand–Prince method that is one of the Runge–Kutta methods in which the integration errors are adaptively controlled within fourth-order accuracy [69]. We also show results of calculations of the Redfield theory for comparison [70–72]. The calculations based on the HEOM theory and the Redfield theory were performed by using the PyHEOM library [21]. All of the calculations were performed using double precision floating point numbers.

A. Vibronic wavepacket dynamics

In this section, we consider a system in which two electronic states are strongly coupled to a single harmonic oscillator. Bath modes are coupled to the oscillator, which causes damped vibration in its time evolution. The total

Hamiltonian is given as

$$\begin{aligned} \hat{H}^{\text{tot}} = & \left(E_0 + \frac{\hbar\omega^{\text{vib}}}{2} (\hat{z} - d_0)^2 \right) |0\rangle\langle 0| \\ & + \left(E_1 + \frac{\hbar\omega^{\text{vib}}}{2} (\hat{z} - d_1)^2 \right) |1\rangle\langle 1| \\ & + J (|0\rangle\langle 1| + |1\rangle\langle 0|) \\ & + \frac{\hbar\omega^{\text{vib}}}{2} \hat{p}^2 + \sum_{\xi} \frac{\hbar\omega_{\xi}}{2} \left[\hat{p}_{\xi}^2 + \left(\hat{x}_{\xi} - \frac{g_{\xi}}{\omega_{\xi}} \hat{z} \right)^2 \right]. \end{aligned} \quad (67)$$

Here, $|0\rangle$ and $|1\rangle$ denote the electronic diabatic states, E_0 and E_1 are stable equilibrium energies of each state, and J is the diabatic coupling between the two states. The operators \hat{z} and \hat{p} are the dimensionless coordinate and conjugate momentum of the system oscillator, respectively, and ω^{vib} is its characteristic frequency. The stable points of \hat{z} in each electronic states are different, d_0 for $|0\rangle$ and d_1 for $|1\rangle$, and therefore the electronic and vibrational states are coupled. We assume the Drude spectral density defined as

$$\mathcal{J}(\omega) = \frac{\zeta}{\omega^{\text{vib}}} \frac{\gamma^{\text{D}2}}{\omega^2 + \gamma^{\text{D}2}}, \quad (68)$$

i.e., $\eta = \zeta\gamma^{\text{D}}/2\omega^{\text{vib}}$, where ζ is the coupling strength between the system oscillator and bath, and $1/\gamma^{\text{D}}$ is the timescale of the bath response function. In the white limit $\gamma^{\text{D}} \rightarrow \infty$, The conditions $\zeta < 2\omega^{\text{vib}}$, $\zeta = 2\omega^{\text{vib}}$, and $\zeta > 2\omega^{\text{vib}}$ correspond to the underdamped, critically damped, and overdamped cases of the oscillator, respectively. This modeling is typical for many photoisomerization processes, and similar models are used in papers [6, 8, 73].

In our calculations, we treat vibrational states of \hat{z} explicitly by using vibrational eigenfunctions on each diabatic state; The wavefunction of the system is expressed as a linear combination of $|j\rangle \otimes |\psi_{a;j}^{\text{vib}}\rangle$, where $|\psi_{a;j}^{\text{vib}}\rangle$ is the a th vibrational eigenfunction on $|j\rangle$,

$$\langle z | \psi_{a;j}^{\text{vib}} \rangle = \frac{1}{\sqrt{2^a a!} \sqrt{\pi}} H_a(z - d_j) \exp\left(-\frac{1}{2}(z - d_j)^2\right), \quad (69)$$

where $H_a(z) = (-1)^a e^{z^2} \partial_z^a e^{-z^2}$ is the a th Hermite polynomial. We introduce the ladder operators acting on $|\psi_{a;j}^{\text{vib}}\rangle$:

$$\hat{c}_j^+ |\psi_{a;j}^{\text{vib}}\rangle = \sqrt{a+1} |\psi_{a;j+1}^{\text{vib}}\rangle \quad (70)$$

and

$$\hat{c}_j^- |\psi_{a;j}^{\text{vib}}\rangle = \sqrt{a} |\psi_{a;j-1}^{\text{vib}}\rangle. \quad (71)$$

Then \hat{z} and \hat{p} can be rewritten as

$$\hat{z} = \frac{1}{\sqrt{2}} (\hat{c}_j^+ + \hat{c}_j^-) + d_j \quad (72)$$

and

$$\hat{p} = \frac{i}{\sqrt{2}} (\hat{c}_j^+ - \hat{c}_j^-), \quad (73)$$

respectively. Thus, the total Hamiltonian is expressed as

$$\hat{H}^{\text{tot}} = \hat{H} + \hat{H}^{\text{int}} + \hat{H}^{\text{bath}} + \hat{H}^{\text{c}}, \quad (74)$$

where

$$\begin{aligned} \hat{H} = & \sum_{j=0,1} \left[E_j + \hbar\omega^{\text{vib}} \left(\hat{c}_j^+ \hat{c}_j^- + \frac{1}{2} \right) \right] |j\rangle\langle j| \\ & + J (|0\rangle\langle 1| + |1\rangle\langle 0|), \end{aligned} \quad (75a)$$

$$\hat{H}^{\text{int}} = -\hat{V} \sum_{\xi} \hbar g_{\xi} \hat{x}_{\xi}, \quad (75b)$$

$$\hat{H}^{\text{bath}} = \sum_{\xi} \frac{\hbar\omega_{\xi}}{2} (\hat{p}_{\xi}^2 + \hat{x}_{\xi}^2), \quad (75c)$$

$$\hat{H}^{\text{c}} = \sum_{\xi} \frac{\hbar g_{\xi}^2}{2\omega_{\xi}} \hat{V}^2, \quad (75d)$$

and

$$\hat{V} = \hat{z} = \sum_{j=0,1} \left[\frac{1}{\sqrt{2}} (\hat{c}_j^+ + \hat{c}_j^-) + d_j \right] |j\rangle\langle j|. \quad (76)$$

The last term in Eq. (74), \hat{H}^{c} , is the so-called counter term [49]. Note that, in order to express the diabatic coupling term $\propto J$ in terms of basis set $\{|\psi_{a;j}^{\text{vib}}\rangle\}$, we need to evaluate the overlap integral $\langle \psi_{a;0}^{\text{vib}} | \psi_{b;1}^{\text{vib}} \rangle$ which is expressed

$$\begin{aligned} \langle \psi_{a;j}^{\text{vib}} | \psi_{b;k}^{\text{vib}} \rangle = & \exp\left(-\frac{d_{jk}^2}{4}\right) \\ & \times \begin{cases} \sqrt{\frac{2^b b!}{2^a a!}} (-d_{jk})^{a-b} L_b^{(a-b)}\left(\frac{d_{jk}^2}{2}\right) & (a \geq b) \\ \sqrt{\frac{2^a a!}{2^b b!}} (+d_{jk})^{b-a} L_a^{(b-a)}\left(\frac{d_{jk}^2}{2}\right) & (a \leq b) \end{cases}, \end{aligned} \quad (77)$$

where $d_{jk} \equiv d_j - d_k$ and we have introduced the associated Laguerre polynomials defined as $L_n^{(\alpha)}(x) \equiv x^{-\alpha} e^x \partial_x^n (e^{-x} x^{x+\alpha})/n!$.

In our calculations, we set the parameters as $E_0 = 2$, $E_1 = 0$, $d_0 = 0$, $d_1 = 4$, and $J = 0.8$. We assume that the initial wavepacket $\psi_i(z)$ at $t = 0$ is the vibrational ground state centered at $d_i = -2$ on $|0\rangle$. In Fig. 1(a), the corresponding diabatic and adiabatic potential energy surfaces (PESs) are illustrated. Bath parameters are $T = 1$, $\gamma^{\text{D}} = 1$, and the coupling strength ζ is chosen from 0.1, 0.5, and 2.5. In Fig. 1(b), the time dependencies of the vibrational response function $\Phi^{\text{vib}}(t)$ under the above conditions are depicted. Note that, even in

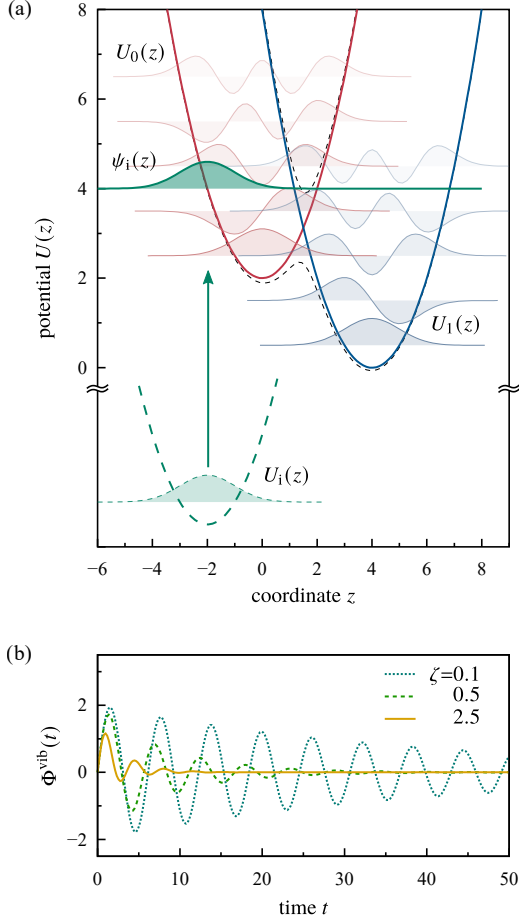


FIG. 1. (a) The PESs of our vibronic model system. The red and solid blue curves represent the diabatic PESs for $|0\rangle$ and $|1\rangle$, respectively. Here, $U_j(z) = \hbar\omega^{\text{vib}}(z - d_j)^2/2$ ($j = 0, 1$). The corresponding adiabatic PESs are depicted as black dashed curves. The first five vibrational eigenfunctions on each diabatic surface are also depicted as thin curves. The solid green curve represents the initial wavepacket $\psi_i(z)$. (b) The vibrational response function of the system oscillator z without electronic coupling. The dotted, dashed, and solid curves represent $\zeta = 0.1, 0.5$, and 2.5 , respectively.

the strong coupling case ($\zeta = 2.5$), the oscillator shows underdamped dynamics.

It is important that, $\hat{V} = \hat{z}$ is expressed in the basis set $|\psi_{a;j}^{\text{vib}}\rangle$ as

$$\hat{V} = \sum_{j=0,1} |\psi_{a;j}^{\text{vib}}\rangle (\mathbf{V}_j)_{ab} \langle \psi_{b;j}^{\text{vib}}|, \quad (78)$$

where

$$\mathbf{V}_j = \frac{1}{\sqrt{2}} \begin{pmatrix} d_j & \sqrt{1} & 0 & \dots & 0 \\ \sqrt{1} & d_j & \sqrt{2} & \ddots & \vdots \\ 0 & \sqrt{2} & \ddots & \ddots & 0 \\ \vdots & \ddots & \ddots & d_j & \sqrt{N^{\text{vib}}-1} \\ 0 & \dots & 0 & \sqrt{N^{\text{vib}}-1} & d_j \end{pmatrix}. \quad (79)$$

Here, N^{vib} is the number of vibrational states on each electronic state we employ. This expression indicates that the effective coupling between the system and bath becomes strong if we employ a large number of vibrational basis functions. In the case of large d_{jk} , the electronic transition between $|j\rangle$ and $|k\rangle$ causes much of vibrational excitations, which requires large N^{vib} to give an accurate description. Even when the system-bath coupling strength ζ itself is not large, this \hat{V} can cause a strong non-perturbative regime.

In Fig. 2, populations of the vibrational ground state on $|0\rangle$, $|\psi_{a;j}^{\text{vib}}\rangle \otimes |j\rangle$, as a function of time t are depicted for (a) weak, moderate, and strong coupling cases ($\zeta = 0.1, 0.5$, and 2.5 , respectively). We performed simulations by using our new treatment (Eq. (54)), the HEOM (Eq. (30)), and the Redfield equations. We truncated the number of vibrational states on each electronic state by $N^{\text{vib}} = 20$. We employed the PSD[1/1] scheme to obtain the parameters of Eq. (23), which causes $K^{\text{BE}} = 1$, $\nu^{(0)} = 6.481$, $\alpha^{(0)} = 1.225$, $m^{(0)} = 1$, and $\Delta = 0.025$. In all the calculations of Eq. (54) here, we set $\omega^f = 1$ and employed a uniform mesh to evaluate differential operation in the q direction, and the mesh range was set $-24 \leq q < +24$ with mesh size $N_q = 64$. The finite difference calculations for q derivative in Eq. (54) were performed using the central difference method with sixth-order accuracy. The values of \mathcal{N}^{max} for Eqs. (54) and (30) and the required computational memories to treat hierarchical elements are given in Table I. In the case of the Redfield equation, in order to keep the equation up to the second-order in the system-bath interaction, we evaluated the Redfield tensor in the eigenspace of \hat{H} instead of $\hat{H} + \hat{H}^c$.

In Fig. 2(a), the results of all the theories are almost coincident because the Born and Markov approximations in the Redfield theory are valid when the coupling is sufficiently small. In the case of moderate coupling, Fig. 2(b), the results of the Redfield theory diverge to infinity because the theory is no longer valid. The results of the HEOM calculations are still valid, but the required size of the hierarchy fairly increases. In Fig. 2(c), it is difficult to obtain converged results from the HEOM theory; The strong coupling between the system and bath caused by ζ and \hat{V} requires a huge number of hierarchy elements, and deep hierarchy elements require high precision in numerical calculations: the coefficients of the second and fifth terms in Eq. (30) become too large. In such cases, the HEOM could be no longer solvable within a fixed preci-

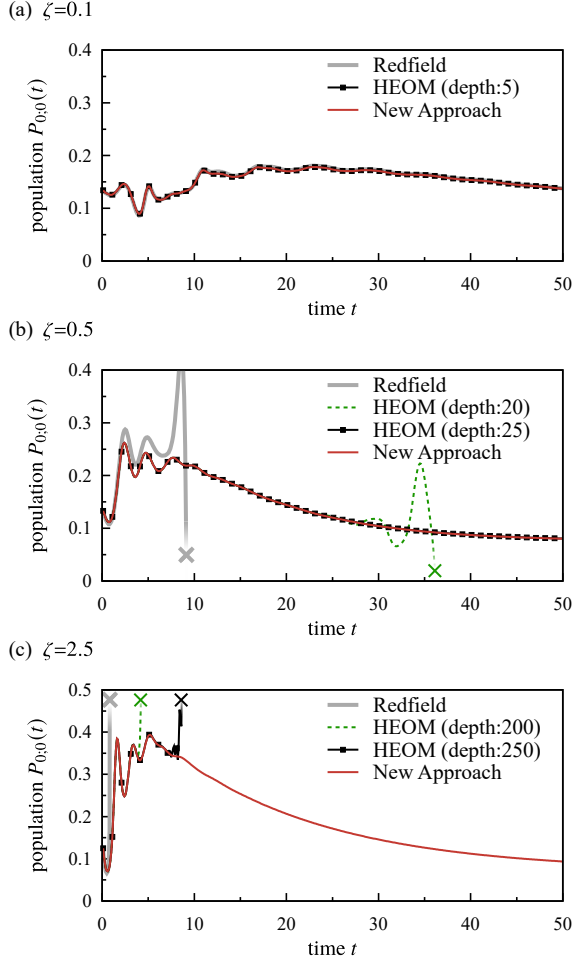


FIG. 2. Populations of the vibrational ground state on $|0\rangle$ as a function of time t , $P_{0,0}(t)$, are depicted for (a) weak, (b) moderate, and (c) strong coupling cases ($\zeta = 0.1, 0.5$, and 2.5 , respectively). The red curves represent the results of Eq. (54), green dashed curves and solid black curves with symbols \blacksquare represent those of the HEOM with different \mathcal{N}^{\max} , and gray thick curves mean those of the Redfield theory. The symbol \times on each line indicates that the calculation diverged to infinity after the point.

TABLE I. The values of \mathcal{N}^{\max} that we employed, and the corresponding size of calculation elements as ratios to the size of the reduced density matrix, $\hat{\rho}(t)$.

Method	\mathcal{N}^{\max}	Size
New Approach	3	256
	5	21
	20	231
	25	351
	250	31,626
Redfield	–	1

sion. Note that, in the case of the HEOM calculations for $\mathcal{N}^{\max} = 250$, we employed the renormalized ADOs defined as $\hat{\rho}'_{\mathbf{n}}(t) \equiv \hat{\rho}_{\mathbf{n}}(t)/\sqrt{\mathbf{n}!}$ in order to suppress a floating point overflow error in deep hierarchy elements [21, 66]. However, this renormalization did not decrease the size of the hierarchy we needed.

It is remarkable that our new treatment, Eq. (54), gives valid results for all the conditions here. This fact can be interpreted as follows; In principle, both Eqs. (30) and (54) are equivalent, and they give the same rigorous results as far as we can evaluate all calculation elements properly. However, when the coupling between the system and bath is strong, a joint distribution of system space and collective bath coordinate space is rather distorted. While Eq. (54) can directly describe such distortion by distribution $\hat{f}(q, \mathbf{x}^{\text{BE}}, t)$, the HEOM (30) treats the distortion within the linear basis expansion (18a). The basis set $\{\psi_{\mathbf{n}}(\mathbf{x})\}$ is optimized to express the uncoupled bath equilibrium state, and therefore it can be inefficient when $\hat{f}(q, \mathbf{x}^{\text{BE}}, t)$ is far from the original equilibrium distribution. In such a case, it is more proper to employ the continuous space representation Eq. (54) instead of Eq. (30). This interpretation also explains why the HEOM is more efficient than our new treatment when the coupling constant is small; In this case, $\hat{f}(q, \mathbf{x}^{\text{BE}}, t)$ is hardly distorted, and hence it can be efficiently expressed by using a small number of basis set Eq. (11).

It is also important that our new treatment requires only a small size of the hierarchy $\{\mathbf{n}^{\text{BE}}\}$ even in the strong coupling case; In Eq. (54), the coupling strength η and \hat{V} do not appear in the terms which connect different hierarchy elements. Hence, the increase of coupling strength hardly increases the value of \mathcal{N}^{\max} which is required to obtain converged results.

In order to examine physics behind the results in Fig. 2, we consider one-dimensional wavepacket in z space, and two-dimensional wavepacket in (z, q) space, defined as

$$f_{jj}(z, t) \equiv \int dq f_{jj}(z, q, t) \quad (80a)$$

and

$$f_{jj}(z, q, t) \equiv \langle z | \otimes \langle j | \hat{f}_{\mathbf{0}}(q, t) | j \rangle \otimes | z \rangle, \quad (80b)$$

respectively. Fig. 3 illustrates the snapshots of wavepackets $f_{jj}(z, t)$ and $f_{jj}(z, q, t)$ for the case $\zeta = 0.5$. At $t = 0$, the wavepacket is located at $z = d_i = -2$, and because we have assumed the factorized initial condition, the joint distribution of the system and collective bath coordinate space, $f_{jj}(z, q, 0)$, is uncorrelated. The wavepacket oscillates according to the PES $U_0(z)$, and it passes the crossing region around $z = z^\dagger = 1.5$ several times. This motion causes non-adiabatic (vibronic) transitions, and hence populations on $|0\rangle \otimes |\psi_{0,0}^{\text{vib}}\rangle$ oscillate around $t = 4$ in Fig. 2(b) and several distinct peaks appear on state $|1\rangle$ in Figs. 3(a-ii) and 3(b-ii). Here,

$$z^\dagger \equiv \frac{(E_1 - E_0)}{\hbar\omega^{\text{vib}}(d_1 - d_0)} + \frac{d_0 + d_1}{2}. \quad (81)$$

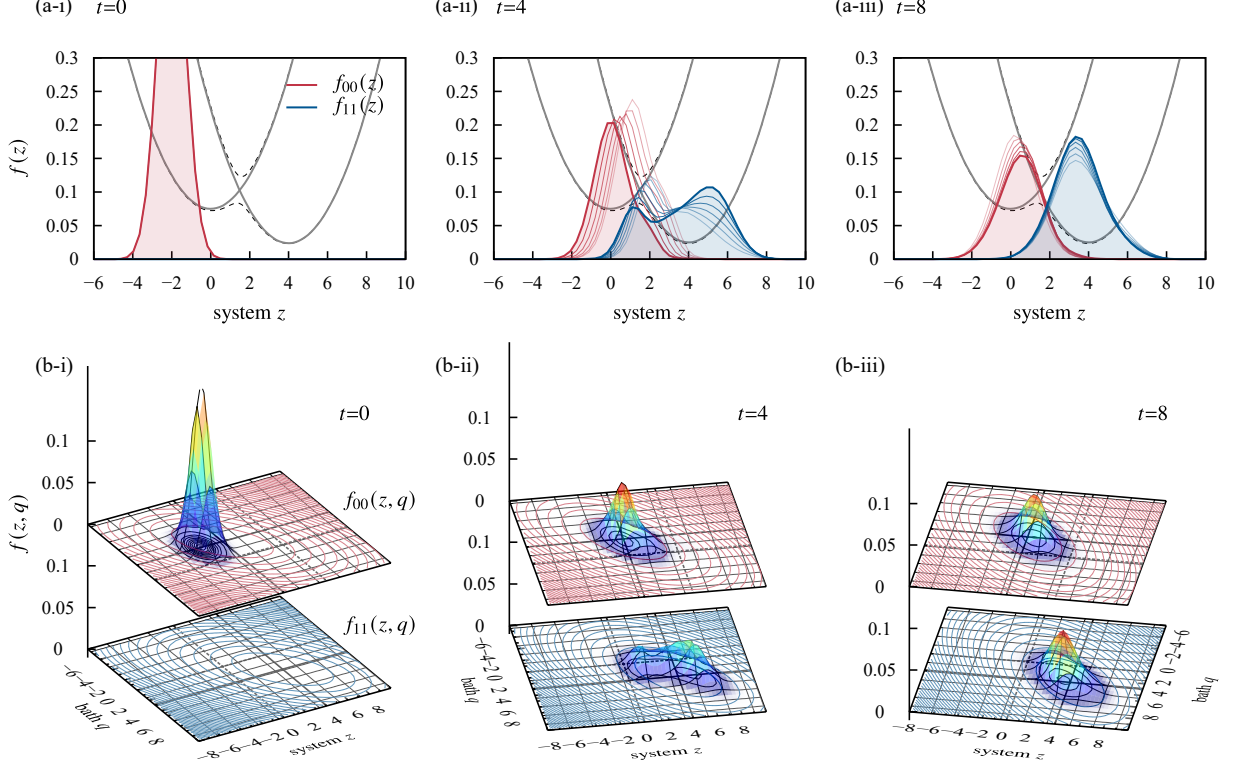


FIG. 3. (a) Snapshots of wavepackets in system space, $f_{jj}(z, t)$, with waiting times (i) $t = 0$, (ii) 4, and (iii) 8. The thick red curves and blue curves represent the wavepackets on $|0\rangle$ and $|1\rangle$ at each time, respectively, and the thin curves represent snapshots for a few time steps before, which are drawn to represent motion of the wavepackets. (b) Snapshots of wavepackets in two-dimensional system-bath space, $f_{jj}(z, q, t)$, with waiting times (i) $t = 0$, (ii) 4, and (iii) 8. The contours of the diabatic PESs are represented by the red and blue contours in the two-dimensional plates for $|0\rangle$ and $|1\rangle$, respectively.

The distribution on the bath coordinate q reorganizes after these non-adiabatic transitions. To make this point clear, we plotted the diabatic PESs corresponding to the extended Hamiltonian, (50), as contours in Fig. 3(b). They are defined as

$$\begin{aligned}
 U_j(z, q) &\equiv E_j + \frac{\hbar\omega^{\text{vib}}}{2} (z - d_j)^2 - \hbar g^f z q + \frac{\hbar\omega^f}{2} q^2 + H^c \\
 &= E_j + \frac{\hbar\omega^{\text{vib}}}{2} (z - d_j)^2 + \frac{\hbar\omega^f}{2} \left(q - \frac{g^f}{\omega^f} z \right)^2.
 \end{aligned}
 \tag{82}$$

This extended PES indicates that the j th diabatic PESs causes reorganization of bath coordinate q to $q = d_j^q$, where

$$d_j^q = \frac{g^f d_j}{\omega^f} = \frac{\sqrt{\gamma^{\text{D}} \zeta} d_j}{\omega^f},
 \tag{83}$$

whose value is $d_0^q = 0$ for $|0\rangle$ and $d_1^q = 2\sqrt{2} \simeq 2.828$ for $|1\rangle$. After time evolution for a certain period, the oscillation on the state $|0\rangle$ is damped, and the wavepacket on $|0\rangle$ becomes trapped at the minimum on the corresponding

adiabatic energy surface (Figs. 3(a-iii) and 3(b-iii)). This trapping causes gradual time evolution of populations in Fig. 2(b).

Thus, the new approach Eq. (54) gives robust calculations and also gives bath space information regarding system state transitions.

B. Spontaneous de-excitation under near zero-temperature environment

As another example, we discuss a spontaneous de-excitation process of a two-level system $\{|g\rangle, |e\rangle\}$ caused by a near zero-temperature bosonic environment. Here, we assume that the Hamiltonian of the system and the system-bath interaction operator are expressed as $\hat{H} = \hbar\Omega_e \hat{c}^+ \hat{c}^-$ and $\hat{V} = \hat{c}^+ + \hat{c}^-$, respectively, where $\hat{c}^+ \equiv |e\rangle\langle g|$ and $\hat{c}^- \equiv |g\rangle\langle e|$ are creation/annihilation operators of the system. To show that our approach is valid for the FSD scheme, which has several higher-order poles $m^{(\xi)} \geq 2$, we set $T = 10^{-2}$ and employed the PSD[1/1]+FSD[6] scheme with the reference tem-

TABLE II. The parameters in Eq. (23) that we employed to evaluate the Bose-Einstein distribution for $T = 10^{-2}$.

	$\xi = 0$	1	2	3
$\nu^{(\xi)}$	6.481	0.7381	0.1815	1.806
$\alpha^{(\xi)}$	122.5	49.55	7.990	-87.20
$m^{(\xi)}$	1	1	2	3
Δ	0.00025			

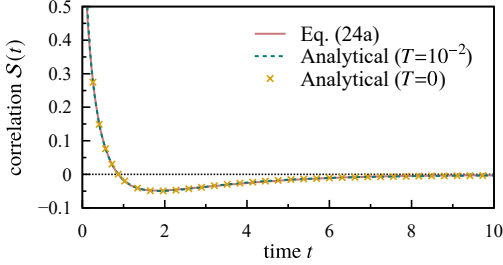


FIG. 4. Symmetrized correlation function $\mathcal{S}(t)$ in the case of $\zeta = 0.5$ and $T = 10^{-2}$ with a Drude spectral density Eq. (22). Solid red and dashed green curves represent Eq. (24a) and analytical evaluation, respectively. The \times symbols depict $\mathcal{S}(t)$ for the zero-temperature limit $T \rightarrow 0$.

perature $T_0 = 1$, which means that the Bose-Einstein distribution function at T_0 is evaluated by the PSD[1/1] scheme and the rest part caused by the difference $T - T_0$ is evaluated by the FSD scheme. This causes $K^{\text{BE}} = 7$, and the results of this parametrization scheme is shown in Table II. In Fig. (4), we plotted $\mathcal{S}(t)$ to check the accuracy of the expansion and the validity of matrix evaluation of poles, Eq. (24a). We set the initial state of the system as the pure excited state $\hat{\rho}(t_0) = |e\rangle\langle e|$, and calculate population dynamics connected to near zero-temperature bath $T = 10^{-2}$. In this model, transitions among the two states are purely caused by the fluctuation of the bath coordinates. Because there is no thermal fluctuation in the zero-temperature limit, the spontaneous transition is dominated by quantum fluctuations of the environment.

In all the calculations of Eq. (54) in this section, we set $\omega^f = 1$ and employed a uniform mesh to evaluate differential operation in the q direction, and the mesh range was set $-12 \leq q < +12$ with mesh size $N_q = 128$. The finite difference calculations for q derivative in Eq. (54) were performed using the central difference method with sixth-order accuracy. Because the large constants $\alpha^{(\xi)}$ in Table II cause strong connections between the hierarchy elements in Eq. (54), we need a deeper hierarchy subspace. The values of \mathcal{N}^{max} for Eqs. (54) and (30) and the required computational memories to treat hierarchical elements are given in Table III. Because the dimension of \mathbf{n}^{BE} is seven, increase of \mathcal{N}^{max} causes a serious increase of the size of hierarchy.

In Fig. (5), we depict the numerical results of the spontaneous de-excitation of the excited state population in

TABLE III. The values of \mathcal{N}^{max} that we employed, and the corresponding size of calculation elements as ratios to the size of the reduced density matrix, $\hat{\rho}(t)$.

Method	\mathcal{N}^{max}	Size
New Approach	9	1,464,320
	2	45
	7	6,435
	20	3,108,105
HEOM	25	13,884,156
	–	1

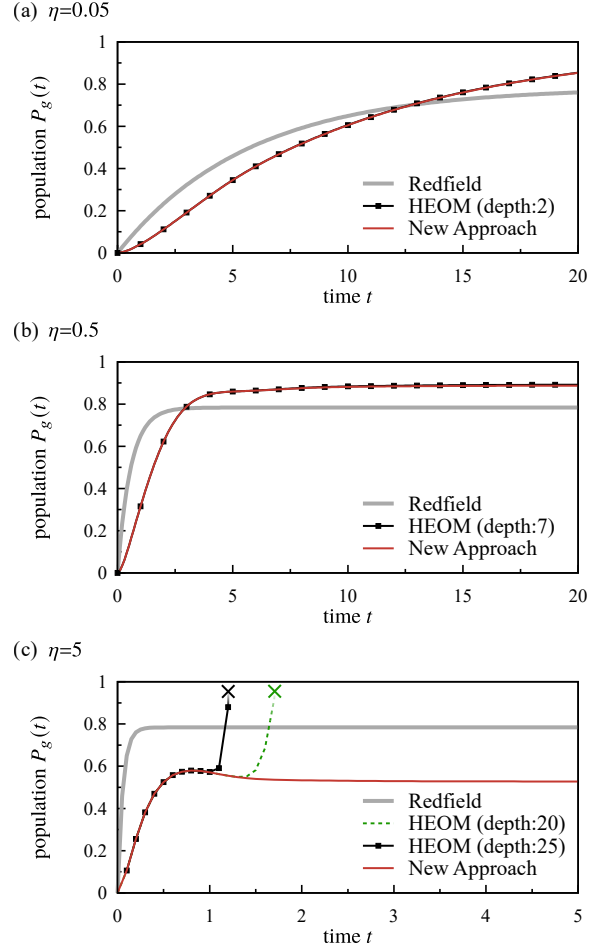


FIG. 5. Populations of the ground state on $|g\rangle$ as a function of time t , $P_g(t)$, are depicted for (a) weak, (b) moderate, and (c) strong coupling cases ($\eta = 0.05$, 0.5 , and $\eta = 5$, respectively). The red curves represent the results of Eq. (54), green dashed curves and solid black curves with symbols \blacksquare represent those of the HEOM with different \mathcal{N}^{max} , and gray thick curves mean those of the Redfield theory. The symbol \times on each line indicates that the calculation diverged to infinity after the point.

the case of weak, moderate, and strong coupling cases ($\eta = 0.05, 0.5, \text{ and } 5$). The parameters were set to $\Omega_0 = 1$ and $\gamma^D = 1$, and the scaling constant ω^f in Eq. (54) was chosen to be $\omega^f = 1$.

In Fig. 5(a), the results of the Redfield theory and other calculations are already different even though it is in a weak coupling regime; Because only \hat{V} causes the spontaneous de-excitation in this model, non-Markovian nature of the bath correlation functions is more important than the model in the previous section, and we cannot employ the Markovian approximation which is included in the Redfield theory [21].

In the cases of Figs. 5(a) and 5(b), the results of Eq. (54) show great agreement with the HEOM results. However, we could not perform convergent HEOM calculations for the case of strong coupling, 5(c). While the situation is similar to the case in Fig. 2 in the previous section, the hierarchy of the HEOM theory required in this parameter is further numerically demanding because \mathbf{n}^{BE} here has a higher dimension. It is interesting that the HEOM calculation for the deeper hierarchy ($\mathcal{N}^{\text{max}} = 25$) shows a severe divergence than that for the shallower hierarchy ($\mathcal{N}^{\text{max}} = 20$) in the strong coupling case. Because a deep hierarchy requires high-precision calculations, an increase of \mathcal{N}^{max} could cause unsolvable equations before we get converged results. As discussed in the previous section, our new approach Eq. (54) gives the exact solution even if the system-bath coupling strength gets beyond the regime that the HEOM theory can practically handle. That the values of equilibrium population $P_g(\infty)$ approaches 0.5 as the coupling strength η increases; Because the system Hamiltonian \hat{H} could be ignorable in the strong coupling limit $\eta \rightarrow \infty$, the population approaches 0.5 asymptotically.

IV. CONCLUDING REMARKS

In this paper, we developed a new approach to treat exact open quantum dynamics coupled to harmonic environments. The approach is derived from the HEOM theory and corresponds to a bath collective coordinate mapping approach in the ‘‘hierarchy’’ space. This treatment is more robust than the HEOM theory and can treat ultra-strong coupling cases in which the size of the hierarchy in the HEOM theory becomes numerous and gets beyond the limits of computational resources. We demonstrated our new approach by using two examples, which clearly show the pros and cons of our approach.

In this paper, we have treated only the case of Drude spectral densities, which causes the Smoluchowski type quantum Fokker–Planck equation [45]. To treat more general spectral densities, we need to extend the bath collective coordinate space into a phase space, which causes the Kramers type quantum Fokker–Planck equations [18, 45, 49–52]. This extension needs a little bit different treatments in the mapping transformation Eq. (35), which will be shown in our next papers.

In this paper, we solved Eq. (54) using the traditional finite difference scheme to make structures of calculations simple. More advanced schemes for Eqs. (54) and (58), such as the discrete variable representation [74] and the time-dependent density matrix renormalization group method [75–79] could be more efficient and handy. Reconstruction of the hierarchical form by using another set of basis functions may have theoretical advantages for strong coupling cases. These problems are left for future investigations.

ACKNOWLEDGMENTS

This work was supported by JSPS KAKENHI Grant No. JP20K22520. Part of the calculations was performed on supercomputers at RCCS (Okazaki), RIIT (Kyushu Univ.), and MASAMUNE-IMR (Tohoku Univ., Project No. 202012-SCKXX-0012).

DATA AVAILABILITY

The data that support the findings of this study are available from the corresponding author upon reasonable request.

Appendix A: Multi-dimensional Hermite polynomials

Our ‘‘basis functions’’ introduced in Eq. (11) can be rewritten as

$$\psi_{\mathbf{n}}(\mathbf{x}) = \frac{1}{\sqrt{2^{|\mathbf{n}|}\pi^{|\mathbf{D}|}}} \bar{H}_{\mathbf{n}}(\mathbf{x}) \exp(-\mathbf{x}^T \mathbf{D}^{-1} \mathbf{x}), \quad (\text{A1})$$

where $\bar{H}_{\mathbf{n}}(\mathbf{x})$ is a multi-dimensional polynomial defined as

$$\begin{aligned} \bar{H}_{\mathbf{n}}(\mathbf{x}) &\equiv (-1)^{|\mathbf{n}|} \exp(\mathbf{x}^T \mathbf{D}^{-1} \mathbf{x}) \\ &\times \left(\mathbf{B}^T \mathbf{D}^{1/2} \partial_{\mathbf{x}} \right)^{\mathbf{n}} \exp(-\mathbf{x}^T \mathbf{D}^{-1} \mathbf{x}). \end{aligned} \quad (\text{A2})$$

The generating function of the set of these polynomials is

$$\sum_{\mathbf{n}} \bar{H}_{\mathbf{n}}(\mathbf{x}) \frac{t^{\mathbf{n}}}{\mathbf{n}!} = \exp \left[t^T \mathbf{B}^T \left(2\mathbf{D}^{-1/2} \mathbf{x} - \mathbf{B}t \right) \right], \quad (\text{A3})$$

and the set satisfies the following recurrence relations:

$$\begin{aligned} x_j \bar{H}_{\mathbf{n}}(\mathbf{x}) &= \frac{1}{2} \sum_k \left(\mathbf{D}^{1/2} \mathbf{B}^T \right)_{jk} \bar{H}_{\mathbf{n}+\mathbf{e}_k}(\mathbf{x}) \\ &+ \sum_k \left(\mathbf{D}^{1/2} \mathbf{B} \right)_{jk} n_k \bar{H}_{\mathbf{n}-\mathbf{e}_k}(\mathbf{x}) \end{aligned} \quad (\text{A4a})$$

and

$$\partial_j \bar{H}_{\mathbf{n}}(\mathbf{x}) = 2 \sum_k \left(\mathbf{D}^{-1/2} \mathbf{B} \right)_{jk} n_k \bar{H}_{\mathbf{n}-\mathbf{e}_k}(\mathbf{x}). \quad (\text{A4b})$$

These polynomials are orthogonal:

$$\begin{aligned} & \int d\mathbf{x} \bar{H}_{\mathbf{n}}(\mathbf{x}) \bar{H}_{\mathbf{n}'}(\mathbf{x}) \exp(-\mathbf{x}^T \mathbf{D}^{-1} \mathbf{x}) \\ &= \sqrt{\pi} 2^{|\mathbf{n}|} |\mathbf{n}|! |\mathbf{D}| \delta_{\mathbf{n}, \mathbf{n}'}. \end{aligned} \quad (\text{A5})$$

Clearly, $\bar{H}_{\mathbf{n}}(\mathbf{x})$ is an extension of the *physicist's Hermite polynomials*, which are characterized by

$$H_n(x) \equiv (-1)^n \exp(x^2) \partial_x^n \exp(-x^2), \quad (\text{A6})$$

$$\sum_n H_n(x) \frac{t^n}{n!} = \exp[t(2xt - t)], \quad (\text{A7})$$

$$xH_n(x) = \frac{1}{2}H_{n+1}(x) + nH_{n-1}(x), \quad (\text{A8a})$$

$$\partial_x H_n(x) = 2nH_{n-1}(x), \quad (\text{A8b})$$

and

$$\int dx H_n(\mathbf{x}) H_{\mathbf{n}'}(\mathbf{x}) \exp(-x^2) = \sqrt{\pi} 2^{|\mathbf{n}|} |\mathbf{n}|! \delta_{\mathbf{n}, \mathbf{n}'}. \quad (\text{A9})$$

The polynomials $\bar{H}_{\mathbf{n}}(\mathbf{x})$ relate to the ordinary multi-dimensional Hermite polynomials $H_{\mathbf{n}}^{[\mathbf{C}]}(\mathbf{x})$ [80] as

$$\bar{H}_{\mathbf{n}}(\mathbf{x}) = H_{\mathbf{n}}^{[2\mathbf{B}^T \mathbf{B}]}(\mathbf{B}^{-1} \mathbf{D}^{-1/2} \mathbf{x}), \quad (\text{A10})$$

where $H_{\mathbf{n}}^{[\mathbf{C}]}(\mathbf{x})$ is defined as

$$H_{\mathbf{n}}^{[\mathbf{C}]}(\mathbf{x}) \equiv (-1)^{|\mathbf{n}|} \exp\left(\frac{1}{2} \mathbf{x}^T \mathbf{C} \mathbf{x}\right) \partial_{\mathbf{x}}^{\mathbf{n}} \exp\left(-\frac{1}{2} \mathbf{x}^T \mathbf{C} \mathbf{x}\right). \quad (\text{A11})$$

Appendix B: Evaluation of the residues for higher-order poles

In this section, we give an evaluation formula of the residue for higher-order poles in a matrix form, which is useful to evaluate bath correlation functions, Eqs. (6a) and (6b).

We assume that a function $f(z)$ has a pole of m th order at $z = C$, i.e.,

$$f(z) = \frac{\tilde{f}(z)}{(z - C)^m}, \quad (\text{B1})$$

where $\tilde{f}(z)$ is a holomorphic function in a neighborhood of C . Usually, the residue of f around $z = C$ is evaluated as

$$\text{Res}_f(C) \equiv \frac{1}{(m-1)!} \lim_{z \rightarrow C} \frac{d^{m-1}}{dz^{m-1}} \tilde{f}(z). \quad (\text{B2})$$

We introduce a $m \times m$ matrix $\tilde{\mathbf{C}}$, which is defined as

$$\tilde{\mathbf{C}} \equiv c \begin{pmatrix} 1 & 0 & \dots & 0 \\ -1 & 1 & 0 & \ddots \\ 0 & \ddots & \ddots & 0 \\ \vdots & \ddots & \ddots & 1 \\ 0 & \dots & 0 & -1 & 1 \end{pmatrix}, \quad (\text{B3a})$$

i.e.,

$$\left(\tilde{\mathbf{C}}\right)_{jk} = c(\delta_{j,k} - \delta_{j,k+1}). \quad (1 \leq j, k \leq m) \quad (\text{B3b})$$

This matrix satisfies

$$\left[\left(\tilde{\mathbf{C}} - c\right)^r\right]_{jk} = (-c)^r \delta_{j,k+r}, \quad (\text{B4})$$

and therefore

$$\mathbf{e}_m^T \left(\tilde{\mathbf{C}} - c\right)^r \mathbf{e}_1 = (-c)^{m-1} \delta_{m-1,r}. \quad (\text{B5})$$

By using the above relations, we obtain

$$\begin{aligned} \text{Res}_f(C) &= \frac{1}{(m-1)!} \lim_{z \rightarrow C} \frac{d^{m-1}}{dz^{m-1}} \tilde{f}(z) \sum_{r=0}^{m-1} \delta_{m-1,r} \\ &= \frac{1}{(-c)^{m-1}} \lim_{z \rightarrow C} \mathbf{e}_m^T \sum_{r=0}^{m-1} \frac{1}{r!} \frac{d^r}{dz^r} \tilde{f}(z) \left(\tilde{\mathbf{C}} - c\right)^r \mathbf{e}_1 \\ &= \frac{1}{(-c)^{m-1}} \mathbf{e}_m^T \tilde{f}(\tilde{\mathbf{C}}) \mathbf{e}_1. \end{aligned} \quad (\text{B6})$$

Here, we have used the Buchheim formula [65], which gives the value of a function of a general matrix. In the case of $\tilde{\mathbf{C}}$ whose eigenvalue is c with its multiplicity m , the formula for a function $g(z)$ reduces

$$g(\tilde{\mathbf{C}}) = \lim_{z \rightarrow c} \sum_{r=0}^{m-1} \frac{1}{r!} \frac{d^r}{dz^r} g(z) (\tilde{\mathbf{C}} - c)^r. \quad (\text{B7})$$

Appendix C: Projection to system-bath collective coordinate space

A joint distribution between the system and bath collective coordinate can be evaluated as

$$\hat{f}(x^{\text{D}}, t) \equiv \hat{f}_0(x^{\text{D}}, t) = \int d\mathbf{x}^{\text{BE}} \mathcal{S}^{\text{ren}} \mathcal{S}^{\text{mix}} \tilde{f}(x^{\text{D}}, \mathbf{x}^{\text{BE}}, t), \quad (\text{C1})$$

By substituting Eq. (18a), i.e.,

$$\tilde{f}(x^{\text{D}}, \mathbf{x}^{\text{BE}}, t) = \sum_{\mathbf{n}^{\text{D}}, \mathbf{n}^{\text{BE}}} \hat{\rho}_{\mathbf{n}^{\text{D}}, \mathbf{n}^{\text{BE}}}(t) \psi_{\mathbf{n}^{\text{D}}}(x^{\text{D}}) \psi_{\mathbf{n}^{\text{BE}}}(\mathbf{x}^{\text{BE}}), \quad (\text{C2})$$

we obtain

$$\hat{f}(x^{\text{D}}, t) = \sum_{\mathbf{n}^{\text{D}}, \mathbf{n}^{\text{BE}}} \prod_{\xi} \sigma^{(\xi) \mathbf{n}^{(\xi)}} \hat{\rho}_{\mathbf{n}^{\text{D}}, \mathbf{n}^{\text{BE}}}(t) \Psi_{\mathbf{n}^{\text{D}} + |\mathbf{n}^{\text{BE}}|}(x^{\text{D}}), \quad (\text{C3})$$

where

$$\begin{aligned} \Psi_{\mathbf{n}}(x^{\text{D}}) &\equiv \frac{1}{\sqrt{\pi} (-g^f)^n \left(\sqrt{2D_{[\gamma^{\text{D}]}}^{f\text{BE}}}\right)^{n+1} n!} \\ &\times H_n\left(\frac{x}{\sqrt{2D_{[\gamma^{\text{D}]}}^{f\text{BE}}}}\right) \exp\left(-\frac{1}{2D_{[\gamma^{\text{D}]}^{f\text{BE}}} x^2}\right), \end{aligned} \quad (\text{C4})$$

where $D_{[\gamma^D]}^{f\text{BE}}$ is given in Eq. (64). Clearly, this is an extension of the formula given in Ref. 47 except the scale factor g^f we have introduced to make $q = x^D$ dimensionless; In the case that higher-order poles do not exist, i.e., $m^{(\xi)} = 1$, the above result reduces those in Refs. 27 and 47. In the above derivation, we have used the following formula:

$$\begin{aligned} & \exp(a\partial_x^2) H_n(\sqrt{bx})e^{-bx^2} \\ &= \frac{1}{(\sqrt{1+4ab})^{n+1}} \exp\left(-\frac{b}{1+4ab}x^2\right) H_n\left(\sqrt{\frac{b}{1+4ab}}x\right). \end{aligned} \quad (\text{C5})$$

-
- [1] V. May and O. Kühn, *Charge and Energy Transfer Dynamics in Molecular Systems* (John Wiley & Sons, 2008).
- [2] U. Weiss, *Quantum Dissipative Systems* (World Scientific, 2011) p. 588.
- [3] C. Kreisbeck and T. Kramer, *J. Phys. Chem. Lett.* **3**, 2828 (2012).
- [4] V. I. Prokhorenko, A. Picchiotti, M. Pola, A. G. Dijkstra, and R. J. D. Miller, *J. Phys. Chem. Lett.* **7**, 4445 (2016).
- [5] K. Miyata, Y. Kurashige, K. Watanabe, T. Sugimoto, S. Takahashi, S. Tanaka, J. Takeya, T. Yanai, and Y. Matsumoto, *Nat. Chem.* **9**, 983 (2017).
- [6] G. D. Scholes, G. R. Fleming, L. X. Chen, A. Aspuru-Guzik, A. Buchleitner, D. F. Coker, G. S. Engel, R. van Grondelle, A. Ishizaki, D. M. Jonas, J. S. Lundeen, J. K. McCusker, S. Mukamel, J. P. Ogilvie, A. Olaya-Castro, M. A. Ratner, F. C. Spano, K. B. Whaley, and X. Zhu, *Nature* **543**, 647 (2017).
- [7] G. D. Scholes, *J. Phys. Chem. Lett.* **9**, 1568 (2018).
- [8] S. Rafiq, B. Fu, B. Kudisch, and G. D. Scholes, *Nat. Chem.* **13**, 70 (2021).
- [9] Y. Tanimura and S. Mukamel, *J. Chem. Phys.* **101**, 3049 (1994).
- [10] N. Makri, *Chem. Phys. Lett.* **193**, 435 (1992).
- [11] G. Ilk and N. Makri, *J. Chem. Phys.* **101**, 6708 (1994).
- [12] H. Wang, *J. Chem. Phys.* **113**, 9948 (2000).
- [13] H. Wang and M. Thoss, *J. Phys. Chem. A* **111**, 10369 (2007).
- [14] A. W. Chin, A. Rivas, S. F. Huelga, and M. B. Plenio, *J. Math. Phys.* **51**, 092109 (2010).
- [15] J. Prior, A. W. Chin, S. F. Huelga, and M. B. Plenio, *Phys. Rev. Lett.* **105**, 050404 (2010).
- [16] W. Xie, Y. Xu, L. Zhu, and Q. Shi, *J. Chem. Phys.* **140**, 174105 (2014).
- [17] Y. Tanimura and R. Kubo, *J. Phys. Soc. Jpn.* **58**, 101 (1989).
- [18] Y. Tanimura, *J. Phys. Soc. Jpn.* **75**, 082001 (2006).
- [19] R.-X. Xu, P. Cui, X.-Q. Li, Y. Mo, and Y. Yan, *J. Chem. Phys.* **122**, 041103 (2005).
- [20] Z. Tang, X. Ouyang, Z. Gong, H. Wang, and J. Wu, *J. Chem. Phys.* **143**, 224112 (2015).
- [21] T. Ikeda and G. D. Scholes, *J. Chem. Phys.* **152**, 204101 (2020).
- [22] Y. Tanimura, *J. Chem. Phys.* **153**, 020901 (2020).
- [23] A. Ishizaki and Y. Tanimura, *Chem. Phys.* **347**, 185 (2008).
- [24] Y. Tanimura and A. Ishizaki, *Acc. Chem. Res.* **42**, 1270 (2009).
- [25] A. Kato and Y. Tanimura, *J. Chem. Phys.* **145** (2016), 10.1063/1.4971370, 1609.08783.
- [26] L. Chen, M. F. Gelin, Y. Zhao, and W. Domcke, *J. Phys. Chem. Lett.* **10**, 5873 (2019).
- [27] E. Mangaud, B. Lasorne, O. Atabek, and M. Desouter-Lecomte, *J. Chem. Phys.* **151** (2019), 10.1063/1.5128852.
- [28] H. Takahashi and Y. Tanimura, *J. Phys. Soc. Jpn.* **89**, 1 (2020), 2004.06994.
- [29] J. Zhang, R. Borrelli, and Y. Tanimura, *J. Chem. Phys.* **152**, 214114 (2020), 2005.05699.
- [30] Y. Iwamoto and Y. Tanimura, *J. Comput. Electron.* **20**, 2091 (2021).
- [31] M. Xu, J. T. Stockburger, and J. Ankerhold, *Phys. Rev. B* **103**, 1 (2021), 2012.11942.
- [32] J. E. Subotnik, A. Jain, B. Landry, A. Petit, W. Ouyang, and N. Bellonzi, *Annu. Rev. Phys. Chem.* **67**, 387 (2016).
- [33] N. Lambert, S. Ahmed, M. Cirio, and F. Nori, *Nat. Commun.* **10**, 3721 (2019).
- [34] A. Ishizaki and Y. Tanimura, *J. Phys. Soc. Jpn.* **74**, 3131 (2005).
- [35] J. Hu, M. Luo, F. Jiang, R.-X. Xu, and Y. Yan, *J. Chem. Phys.* **134**, 244106 (2011).
- [36] H.-D. Zhang, L. Cui, H. Gong, R.-X. Xu, X. Zheng, and Y. Yan, *J. Chem. Phys.* **152**, 064107 (2020).
- [37] Y. Tanimura, *Phys. Rev. A* **41**, 6676 (1990).
- [38] Y. Tanimura and S. Mukamel, *J. Phys. Soc. Jpn.* **63**, 66 (1994).
- [39] M. Tanaka and Y. Tanimura, *J. Phys. Soc. Jpn.* **78**, 073802 (2009).
- [40] Y. Tanimura, *J. Chem. Phys.* **137**, 22A550 (2012).
- [41] Y. Fujihashi, G. R. Fleming, and A. Ishizaki, *J. Chem. Phys.* **142**, 212403 (2015).
- [42] I. S. Dunn, R. Tempelaar, and D. R. Reichman, *J. Chem. Phys.* **150**, 184109 (2019).
- [43] A. Garg, J. N. Onuchic, and V. Ambegaokar, *J. Chem. Phys.* **83**, 4491 (1985).
- [44] Q. Shi, L. Chen, G. Nan, R.-X. Xu, and Y. Yan, *J. Chem. Phys.* **130**, 164518 (2009).
- [45] T. Ikeda and Y. Tanimura, *J. Chem. Theory Comput.* **15**, 2517 (2019).
- [46] R. Kapral and G. Ciccotti, *J. Chem. Phys.* **110**, 8919 (1999).
- [47] H. Liu, L. Zhu, S. Bai, and Q. Shi, *J. Chem. Phys.* **140**, 134106 (2014).

- [48] Y. Yan, T. Xing, and Q. Shi, *J. Chem. Phys.* **153** (2020), 10.1063/5.0027962.
- [49] A. O. Caldeira and A. J. Leggett, *Physica A* **121**, 587 (1983).
- [50] Y. Tanimura and P. G. Wolynes, *Phys. Rev. A* **43**, 4131 (1991).
- [51] T. Ikeda and Y. Tanimura, *J. Chem. Phys.* **147**, 014102 (2017).
- [52] T. Ikeda and Y. Tanimura, *Chem. Phys.* **515**, 203 (2018).
- [53] D. Tamascelli, A. Smirne, S. F. Huelga, and M. B. Plenio, *Phys. Rev. Lett.* **120**, 30402 (2018), 1709.03509.
- [54] Y. Tanimura, *J. Chem. Phys.* **141**, 044114 (2014).
- [55] Y. Tanimura, *J. Chem. Phys.* **142**, 144110 (2015).
- [56] H.-D. Zhang, Q. Qiao, R.-X. Xu, X. Zheng, and Y. Yan, *J. Chem. Phys.* **147**, 044105 (2017).
- [57] H. Risken, *The Fokker-Planck Equation*, Vol. 18 (Springer-Verlag, Berlin, 1989).
- [58] T. Ikeda, H. Ito, and Y. Tanimura, *J. Chem. Phys.* **142**, 212421 (2015).
- [59] J. Hu, R.-X. Xu, and Y. Yan, *J. Chem. Phys.* **133**, 101106 (2010).
- [60] L. Cui, H.-D. Zhang, X. Zheng, R.-X. Xu, and Y. Yan, *J. Chem. Phys.* **151**, 024110 (2019).
- [61] A. J. Leggett, *Phys. Rev. B* **30**, 1208 (1984).
- [62] R. Martinazzo, B. Vacchini, K. H. Hughes, and I. Burghardt, *J. Chem. Phys.* **134** (2011), 10.1063/1.3532408.
- [63] M. P. Woods, R. Groux, A. W. Chin, S. F. Huelga, and M. B. Plenio, *J. Math. Phys.* **55**, 32101 (2014), 1111.5262.
- [64] T. Ikeda, A. G. Dijkstra, and Y. Tanimura, *J. Chem. Phys.* **150** (2019), 10.1063/1.5086948.
- [65] R. A. Horn and C. R. Johnson, *Topics in Matrix Analysis* (Cambridge University Press, Cambridge, 1991).
- [66] Q. Shi, L. Chen, G. Nan, R.-X. Xu, and Y. Yan, *J. Chem. Phys.* **130**, 084105 (2009).
- [67] R. Härtle, G. Cohen, D. R. Reichman, and A. J. Millis, *Phys. Rev. B* **88**, 235426 (2013).
- [68] R. Härtle, G. Cohen, D. R. Reichman, and A. J. Millis, *Phys. Rev. B* **92**, 085430 (2015).
- [69] J. R. Dormand and P. J. Prince, *J. Comput. Appl. Math.* **15**, 203 (1986).
- [70] A. G. Redfield, "The theory of relaxation processes," in *Advances in Magnetic and Optical Resonance*, Vol. 1, edited by J. S. Waugh (Academic Press, 1965) pp. 1–32.
- [71] M. Yang and G. R. Fleming, *Chem. Phys.* **275**, 355 (2002).
- [72] A. Ishizaki and G. R. Fleming, *J. Chem. Phys.* **130**, 234110 (2009).
- [73] N. Christensson, H. F. Kauffmann, T. Pullerits, and T. Mančal, *J. Phys. Chem. B* **116**, 7449 (2012).
- [74] D. T. Colbert and W. H. Miller, *J. Chem. Phys.* **96**, 1982 (1992).
- [75] S. R. White, *Phys. Rev. Lett.* **69**, 2863 (1992).
- [76] U. Schollwoeck, *Rev. Mod. Phys.* **77** (2004), 10.1103/RevModPhys.77.259, 0409292.
- [77] G. Vidal, *Phys. Rev. Lett.* **93**, 40502 (2004), 0310089 [quant-ph].
- [78] A. J. Daley, C. Kollath, U. Schollwöck, and G. Vidal, *J. Stat. Mech. Theory Exp.* **2004**, P04005 (2004), 0403313.
- [79] S. R. White and A. E. Feiguin, *Phys. Rev. Lett.* **93**, 1 (2004), 0403310.
- [80] S. Berkowitz and F. J. Garner, *Math. Comput.* **24**, 537 (1970).